


Signal Parameter Estimation for Passive Bistatic Radar With Waveform Correlation Exploitation

FANGZHOU WANG

HONGBIN LI , Senior Member, IEEE

XIN ZHANG , Member, IEEE

Stevens Institute of Technology, Hoboken, NJ USA

BRAHAM HIMED, Fellow, IEEE

Air Force Research Laboratory, Dayton, OH USA

This paper addresses the problem of target delay and Doppler frequency estimation for passive bistatic radar employing noncooperative illuminators of opportunity (IOs), where the receivers are contaminated by nonnegligible noise, clutter, and direct-path interference. A parametric approach is proposed by modeling the unknown signal transmitted from the IO as an autoregressive process whose temporal correlation is jointly estimated and exploited for passive estimation. An iterative estimator based on the expectation-maximization (EM) principle is utilized to solve this highly nonlinear problem. We also discuss the initialization of the EM-based estimator and a fast implementation based on the fast Fourier transform and interpolation techniques. In addition, we derive the Cramér–Rao lower bound for the estimation problem to benchmark the performance of the proposed estimator. Simulation results show that the proposed estimator behaves similarly to a clairvoyant EM estimator, which assumes knowledge of the IO waveform covariance matrix, and significantly outperforms other methods that ignore the waveform correlation.

Manuscript received December 30, 2016; revised June 23, 2017 and October 17, 2017; released for publication October 26, 2017. Date of publication November 20, 2017; date of current version June 7, 2018.

DOI. No. 10.1109/TAES.2017.2775898

Refereeing of this contribution was handled by K. S. Kulpa.

This work was supported in part by a subcontract with Matrix Research, Inc., for research sponsored by the Air Force Research Laboratory and in part by the National Science Foundation under Grant ECCS-1609393.

Authors' addresses: F. Wang, H. Li, and X. Zhang are with the Department of Electrical and Computer Engineering, Stevens Institute of Technology, Hoboken, NJ 07030 USA, E-mail: (fwang11@stevens.edu; Hongbin.Li@stevens.edu; xzhang23@stevens.edu.); B. Himed is with the RF Technology Branch, Air Force Research Laboratory, Dayton, OH 45433 USA, E-mail: (braham.himed@us.af.mil). (*Corresponding author: H. Li.*)

0018-9251 © 2017 IEEE

I. INTRODUCTION

Passive radar, which can detect and track targets of interest by exploiting readily available, noncooperative illuminators of opportunity (IOs), has been attracting significant attention in recent years [1]–[7]. Usable IO sources include frequency modulation (FM) radio, television, digital audio/video broadcasting, cellular signals, and others. Since no transmitters are required in a passive radar, it is more covert and provides lower vulnerability to deliberate interference and reduced pollution to the electromagnetic environment. Furthermore, the bistatic or multistatic configuration of passive radar enables it to obtain spatial diversity of the target's radar cross section, which can lead to improved sensing performance [8]–[10].

Unlike conventional active radar systems, where the transmitted waveforms are carefully designed with desired properties, passive sensing is more challenging due to the noncooperative nature of the IO: the transmitted signal is not only out of control but also generally unknown to the receiver. As a result, the conventional matched filtering (MF) based techniques routinely used in active radar cannot be implemented for estimation and detection in passive radar. One general approach to dealing with the unknown IO waveform is to treat it as a deterministic signal. By employing a reference channel (RC) at the receiver to collect the direct-path (transmitter-to-receiver) signal as an estimate of the IO waveform, the cross-correlation (CC) is a popular passive sensing method that mimics MF [11]–[14]. Specifically, the reference signal, which plays the role of the transmitted signal in the MF, is used to cross-correlate with the target echo in the surveillance channel (SC), a separate channel employed for target detection. However, while the MF is optimum as it maximizes the receiver output signal-to-noise ratio (SNR), the CC is suboptimal due to the noisy reference signal. In fact, it was shown in [15] that the CC is highly sensitive to noise. Recently, [16] and [17] developed improved passive detectors by taking into account the effect of noisy reference. In particular, [16] considered the case when the knowledge of the noise power is known under a multi-input multi-output setup, while [17] examined several cases including when the noise power is unknown.

Another approach to dealing with the unknown IO waveform is to model it as a stochastic process. A simple solution within this category is to treat the samples of the waveform as independent and identically distributed variables, i.e., the waveform correlation is neglected. Two stochastic passive detectors based on this idea were developed in [17] assuming known and unknown noise power. Due to coding, modulation, pulse shaping, propagation effects, etc., the IO waveform is in general correlated and such correlation can be exploited to improve passive sensing performance. Along this line, [18] considered the problem of estimating the delay and Doppler frequency of a target in passive radar by modeling the IO waveform as a correlated Gaussian process with known correlation. In practice, the correlation is unknown and has to be estimated. In addition, the correlation may change over time. Therefore, it would

be of interest to develop techniques that can adaptively estimate the correlation and employ it for passive detection and estimation.

Another challenge in passive sensing is the need to deal with the direct-path interference (DPI) and clutter. The DPI, which refers to the direct transmission from the IO to the passive receiver, is much stronger (by many tens to even over a hundred dB) compared to the target echo [19], [20]. The effect of the DPI on the CC detector was analyzed in [15], which showed that a modest level of DPI can significantly degrade the detection performance of the CC. Meanwhile, the target signal is also dominated by clutter echoes if there are significant stationary objects in the radar scene. As such, passive radar has to employ some interference cancellation, e.g., spatial/temporal adaptive filtering techniques [21]–[25]. Despite such cancellation, some residual DPI and clutter may still exist due to, e.g., limited array size and null depth. As a result, the DPI and clutter may still be at a non-negligible power level compared with the target echo.

In this paper, we examine the target delay and Doppler frequency estimation problem for a passive bistatic radar system, where the receiver is contaminated by non-negligible noise, clutter, and DPI. We propose a parametric approach that models the unknown IO signal as an autoregressive (AR) process, whose temporal correlation is estimated and exploited for target delay and Doppler frequency estimation. Since the maximum likelihood (ML) estimates of the unknown parameters cannot be obtained in closed form, we resort to an expectation-maximization (EM) procedure [26] to find these estimates. The initialization of the EM algorithm is based on a modified cross-correlation (MCC) method involving sequential interference cancellation and CC. In addition, we derive the Cramér–Rao lower bound (CRLB) for the estimation problem to benchmark the performance of the proposed estimator. Extensive simulation results are presented, which show that the proposed EM-AR estimator is close to a clairvoyant EM estimator, which assumes knowledge of the waveform covariance matrix, and significantly outperforms the MCC and an impaired EM estimator, which ignores the waveform correlation.

The remainder of the paper is organized as follows. In Section II, we present the system model and formulate the problem of interest. Section III presents the proposed EM-AR estimator including its initialization, fast implementation based on the fast Fourier transform (FFT) and interpolation, as well as the associated CRLB. Numerical results and discussions are included in Section IV, followed by conclusions in Section V.

Notation: Throughout the paper, scalars are denoted by nonboldface type, vectors (matrices) are denoted by boldface lower (upper) case letters, and all vectors are column vectors. Superscripts $(\cdot)^T$, $(\cdot)^*$, and $(\cdot)^H$ denote transpose, complex conjugate, and complex conjugate transpose, respectively. $\Re\{\cdot\}$ and $\Im\{\cdot\}$ represent the real and imaginary part of a complex quantity, respectively, $E\{\cdot\}$ denotes statistical expectation, and j stands for the imaginary unit. $\mathbf{0}_{p \times q}$

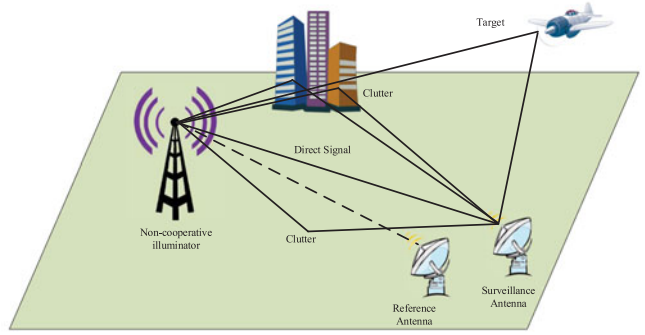


Fig. 1. Passive radar scenario.

denotes a $p \times q$ matrix with all zero entries, \mathbf{I}_N denotes an identity matrix of size N , $[\cdot]_{m,n}$ denotes the (m, n) th entry of a matrix, and $[\cdot]_m$ denotes the m th element of a vector. \odot and \otimes stand for the Hadamard and the Kronecker products, respectively. The notation \mathcal{CN} denotes a circularly symmetric, complex Gaussian distribution. $\det\{\cdot\}$ represents the determinant of a matrix, $\|\cdot\|$ is the Frobenius norm, and $\text{tr}\{\cdot\}$ denotes the trace of a matrix.

II. SIGNAL MODEL

A passive radar geometry is shown in Fig. 1, which consists of a noncooperative IO and two independent antennas. One is the RC antenna, which receives the unknown source signal transmitted directly from the IO, and the other one is the SC antenna, which collects echoes from moving targets of interest due to the illumination of the IO. The RC utilizes a directional antenna steered toward the IO transmitter to collect a copy of the IO waveform, while the surveillance antenna is set up to point in the direction to be surveyed. We assume the SC employs some interference mitigation technique, but residual DPI and clutter are present due to imperfect cancellation (see Section I). The clutter is assumed to be caused by reflections from stationary objects, such as buildings, mountains, and other ground scatters, and has zero Doppler frequency. Given the above-mentioned discussions, the (baseband equivalent) signal in the SC can be written as

$$y'_s(t) = \gamma'_d x'(t - \tau_d) + \sum_{k=1}^{K_t} \alpha'_k x'(t - t_k) e^{j2\pi f_k t} + \sum_{k=1}^{K_c} \beta'_k x'(t - t'_k) + n'_s(t) \quad (1)$$

where γ'_d is the channel coefficient associated with the DPI, $x'(t)$ is the unknown signal transmitted by the IO, τ_d is the propagation delay from the IO to the SC, α'_k is the amplitude of the k th target, t_k is the propagation delay due to the transmission from the IO to the k th target and then from the target to the SC, f_k is the Doppler frequency of the k th target, β'_k is the amplitude of the k th clutter scatterer, t'_k is the associated delay, $n'_s(t)$ is the additive zero-mean white Gaussian noise, and K_t and K_c denote the numbers of targets and clutter components, respectively. In practice,

K_t and K_c can be estimated from the delay-Doppler map of the observed signal.

Meanwhile, the received signal in the RC can be expressed as

$$y'_r(t) = \gamma x'(t - \tau_d) + n'_r(t) \quad (2)$$

where γ is the channel coefficient from the IO to the RC, τ_d is the propagation delay, which is identical to that in (1) since the RC and SC are colocated, and $n'_r(t)$ is the additive zero-mean white Gaussian noise. It is assumed that target and clutter echoes (received by the sidelobes of the reference antenna) are negligible due to the directional reference antenna.

To simplify the system model, we observe that the propagation delay of the DPI τ_d is usually known and can be compensated for, since the location of the IO is known to the passive radar. Let $y_r(t) = y'_r(t + \tau_d)$ and $y_s(t) = y'_s(t + \tau_d)$ denote the delay-compensated signals for the RC and SC, respectively. The delay-compensated noise $n_r(t)$ and $n_s(t)$ are similarly defined. Moreover, since γ and $x'(t)$ are both unknown, they cannot be separately estimated. In the following, γ is absorbed as part of the waveform. This leads to

$$\begin{aligned} y_r(t) &= x(t) + n_r(t), \\ y_s(t) &= \gamma_d x(t) + \sum_{k=1}^{K_t} \alpha_k x(t - \tau_k) e^{j2\pi f_k t} \\ &\quad + \sum_{k=1}^{K_c} \beta_k x(t - \tau'_k) + n_s(t) \end{aligned} \quad (3)$$

where $\tau_k \triangleq t_k - \tau_d$ denotes the bistatic delay for the k th target, $\tau'_k \triangleq t'_k - \tau_d$ the bistatic delay for the k th clutter component, $x(t) \triangleq \gamma x'(t)$, $\gamma_d \triangleq \gamma'_d / \gamma$, $\alpha_k \triangleq \alpha'_k e^{j2\pi f_k \tau_d} / \gamma$, and $\beta_k \triangleq \beta'_k / \gamma$.

We assume that $x(t)$ has a duration of T seconds, e.g., due to framed transmissions employed by the IO, in which case T represents the frame duration. The observation interval T_o is selected such that $T_o \geq T + \tau_{\max}$, where τ_{\max} denotes the maximum bistatic delay that can be tolerated by the system. We sample the RC and SC signals using a sampling frequency $f_s \geq 2(B + f_{\max})$, where B denotes the bandwidth of the communication signal $x(t)$ and f_{\max} is the maximum Doppler frequency of the target that is designed detectable by the system. Suppose M samples are collected over the observation window T_o , i.e., $T_o = MT_s$, where $T_s = 1/f_s$ denotes the sampling interval. Let \mathbf{y}_r , \mathbf{y}_s , \mathbf{x} , \mathbf{n}_r , and \mathbf{n}_s be $M \times 1$ vectors formed by M adjacent samples of $y_r(t)$, $y_s(t)$, $x(t)$, $n_r(t)$, and $n_s(t)$, respectively. The M -point discrete Fourier transform (DFT) matrix \mathbf{T} has entries $[\mathbf{T}]_{p,q} = e^{-j2\pi(p-1)\Delta f(q-1)T_s} / \sqrt{M}$ for $p, q = 1, 2, \dots, M$, with the frequency-domain sample spacing $\Delta f = \frac{f_s}{M} = \frac{1}{T_s M}$, and $\mathbf{W}(x)$ is a diagonal matrix with diagonal entries $[\mathbf{W}(x)]_{p,p} = e^{j2\pi(p-1)x}$ for $p = 1, 2, \dots, M$. Then, with a little notational abuse of τ_k

and f_k , the digitized model can be expressed as [18], [27]

$$\begin{aligned} \mathbf{y}_r &= \mathbf{x} + \mathbf{n}_r, \\ \mathbf{y}_s &= \sum_{k=1}^K \gamma_k \mathcal{D}(\tau_k, f_k) \mathbf{x} + \mathbf{n}_s, \end{aligned} \quad (4)$$

where \mathbf{n}_r and \mathbf{n}_s are mutually independent zero-mean white Gaussian noise with covariance matrices $\sigma_r^2 \mathbf{I}$ and $\sigma_s^2 \mathbf{I}$, respectively. Note that the DPI, target, and clutter signals are combined in one summation in (4) to simplify the notation. Specifically, $k = 1$ refers to the DPI with $\tau_1 = 0$ and $f_1 = 0$, $k = 2, \dots, K_t + 1$ refer to the targets echo with $\tau_k \neq 0$ and $f_k \neq 0$, and $k = K_t + 2, \dots, K$ refer to the clutter components with $\tau_k \neq 0$ but $f_k = 0$. Thus, we have $K = K_t + K_c + 1$. In addition, the unitary matrix $\mathcal{D}(\tau_k, f_k)$ is the delay-Doppler operator:

$$\mathcal{D}(\tau_k, f_k) = \mathbf{W}(f_k T_s) \mathbf{T}^H \mathbf{W}(-\tau_k \Delta f) \mathbf{T} \quad (5)$$

where the rightmost \mathbf{T} converts the signal to the frequency domain, $\mathbf{W}(-\tau_k \Delta f)$ introduces a phase shift (in the frequency domain) caused by the time-domain delay τ_k , the next \mathbf{T}^H converts the signal back to the time domain, and finally, $\mathbf{W}(f_k T_s)$ imposes a phase shift (in the time domain) due to the Doppler frequency f_k .

The IO waveform \mathbf{x} is modeled as an element-correlated stochastic process with unknown temporal correlation. In this paper, we use an AR process to model the stochastic IO waveform, where the temporal correlation is parameterized by the AR coefficients. The AR process can be expressed as

$$x(n) = - \sum_{p=1}^P a(p) x(n-p) + w(n), \quad n = 1, 2, \dots, N \quad (6)$$

where $N = \lfloor \frac{T}{T_s} + 1 \rfloor \leq M$ is the number of the framed IO signal samples, P is the AR model order, $a(p)$ is the p th AR coefficient, with $\mathbf{a} = [a(1), a(2), \dots, a(P)]^T$, and $w(n) \sim \mathcal{CN}(0, \sigma^2)$ denotes the driving noise. Consequently, \mathbf{x} is zero-mean Gaussian distributed with covariance matrix $\mathbf{C}_x(\mathbf{a}, \sigma^2)$, which is Hermitian, Toeplitz, and thus can be fully determined by its first column $\mathbf{r}_{xx} = [r_{xx}(0), r_{xx}(1), \dots, r_{xx}(N-1)]^T$, i.e., the autocorrelation function (ACF) sequence. In addition, the relationship between the AR parameters $\{\mathbf{a}, \sigma^2\}$ and the ACF is described by the Yule-Walker equations [28]

$$r_{xx}(n) = \begin{cases} - \sum_{p=1}^P a(p) r_{xx}(n-p), & n \geq 1, \\ - \sum_{p=1}^P a(p) r_{xx}(-p) + \sigma^2, & n = 0 \end{cases} \quad (7)$$

where $r_{xx}(n) = r_{xx}^*(-n)$.

A comment of the choice of the AR model is in order. It is a simple modeling tool to model the waveform correlation. It is also universal in that any stationary stochastic process under mild conditions can be modeled as an AR process [28]. There is no doubt that there might be some mismatch between the IO signal and the specific AR model used for estimation. In Section IV, we have included simulated IO signals, which are not from AR models, and FM

signals to test the proposed method. Our results indicate that even with mismatch, the AR model still allows us to capture the waveform correlation, leading to improved estimation performance over methods, which completely ignore such correlation.

The problem of interest is to jointly estimate the unknown parameters from the observations \mathbf{y}_r and \mathbf{y}_s in (4). The unknown parameters can be denoted as $\boldsymbol{\theta} = [\mathbf{f}^T, \boldsymbol{\tau}^T, \boldsymbol{\gamma}^T, \boldsymbol{\theta}_{\text{AR}}^T]^T$, where \mathbf{f} contains the Doppler frequencies of the targets, $\boldsymbol{\tau}$ includes the delays of the targets and clutter components, and $\boldsymbol{\theta}_{\text{AR}} = [\mathbf{a}^T, \sigma^2]^T$ collects the AR parameters.

III. PROPOSED METHOD

A. Overview

Given the observations described by (4), one would naturally consider the ML estimator. To simplify the notation, let $\boldsymbol{\Omega}(\mathbf{f}, \boldsymbol{\tau}, \boldsymbol{\gamma}) = \sum_{k=1}^K \gamma_k \mathcal{D}(\tau_k, f_k)$. The surveillance signal in (4) can be simplified as $\mathbf{y}_s = \boldsymbol{\Omega}(\mathbf{f}, \boldsymbol{\tau}, \boldsymbol{\gamma})\mathbf{x} + \mathbf{n}_s$. Under the condition stated in Section II, the observations $\mathbf{y} = [\mathbf{y}_r^T, \mathbf{y}_s^T]^T$ are jointly Gaussian with zero mean and covariance matrix

$$\mathbf{C}_{yy}(\boldsymbol{\theta}) = \begin{bmatrix} \mathbf{C}_{rr} & \mathbf{C}_{rs} \\ \mathbf{C}_{rs}^H & \mathbf{C}_{ss} \end{bmatrix} \quad (8)$$

where $\mathbf{C}_{rr} = \mathbf{C}_x(\mathbf{a}, \sigma^2) + \sigma_r^2 \mathbf{I}$, $\mathbf{C}_{rs} = \boldsymbol{\Omega}(\mathbf{f}, \boldsymbol{\tau}, \boldsymbol{\gamma})\mathbf{C}_x(\mathbf{a}, \sigma^2)$, and $\mathbf{C}_{ss} = \boldsymbol{\Omega}(\mathbf{f}, \boldsymbol{\tau}, \boldsymbol{\gamma})\mathbf{C}_x(\mathbf{a}, \sigma^2)\boldsymbol{\Omega}(\mathbf{f}, \boldsymbol{\tau}, \boldsymbol{\gamma})^H + \sigma_s^2 \mathbf{I}$. The ML estimator is computationally prohibitive since the signal parameters are embedded in the covariance matrix $\mathbf{C}_{yy}(\boldsymbol{\theta})$, which appears as the matrix inverse and determinant in the likelihood function. Instead, we consider the EM approach, which employs the conditional distribution $p(\mathbf{y}|\mathbf{x})$, whereby $\boldsymbol{\Omega}(\mathbf{f}, \boldsymbol{\tau}, \boldsymbol{\gamma})\mathbf{x}$ appears as the mean in the conditional distribution, which makes the resulting cost function easier to optimize. In addition, EM is an iterative algorithm, which updates the unknown parameters in a sequential and readily implementable fashion.

As we shall see, in the iterative process of the EM algorithm, $\boldsymbol{\gamma}$, \mathbf{a} , and σ^2 can be updated in closed form. However, there is no closed-form update for \mathbf{f} and $\boldsymbol{\tau}$. A brute-force search of the delay and Doppler is still computationally intensive. To address this problem, we propose in Section III-C a fast algorithm for delay and Doppler estimation by utilizing the FFT. Furthermore, since the EM algorithm requires initial estimates of the unknown parameters, we discuss an initialization scheme in Section III-D by using an MCC procedure based on successive interference cancellation. Finally, the CRLB was derived to benchmark the performance of the proposed method in Section III-E.

B. EM-Based Estimator

To derive an EM-based solution, we consider the following ‘‘complete’’ data for our problem, which includes the observations $\mathbf{y} = [\mathbf{y}_r^T, \mathbf{y}_s^T]^T$ and the IO waveform \mathbf{x} :

$$\mathbf{z} = [\mathbf{x}^T, \mathbf{y}^T]^T. \quad (9)$$

Next, we need to determine the likelihood function of \mathbf{z} conditioned on the unknown parameters. We use the asymptotic form of the likelihood function for the IO waveform \mathbf{x} [29], which is easier to deal with than the exact likelihood:

$$p(\mathbf{x}) = \frac{1}{(\pi\sigma^2)^{(N-P)}} e^{-\frac{1}{\sigma^2} \sum_{n=p+1}^N |w(n)|^2}. \quad (10)$$

To express the likelihood function explicitly in terms of the IO waveform samples $x(n)$, we define

$$\mathbf{x}_n = [x(n+1), x(n+2), \dots, x(n+N-P)]^T \quad (11)$$

for $n = 0, 1, \dots, P$, and

$$\mathbf{Y} = [\mathbf{x}_{P-1}, \mathbf{x}_{P-2}, \dots, \mathbf{x}_0]. \quad (12)$$

Then, the likelihood function for the IO waveform can be written as

$$p(\mathbf{x}) = \frac{1}{(\pi\sigma^2)^{(N-P)}} e^{-\frac{1}{\sigma^2} \|\mathbf{x}_P + \mathbf{Y}\mathbf{a}\|^2}. \quad (13)$$

Finally, the likelihood function of \mathbf{z} is

$$p(\mathbf{z}|\boldsymbol{\theta}) = p(\mathbf{y}|\mathbf{x}, \boldsymbol{\theta})p(\mathbf{x}|\boldsymbol{\theta}) = \frac{1}{\det(\pi\mathbf{C}_{2M})(\pi\sigma^2)^{(N-P)}} \times \exp \left\{ -\frac{1}{\sigma^2} \|\mathbf{x}_P + \mathbf{Y}\mathbf{a}\|^2 - \frac{1}{\sigma_r^2} \|\mathbf{y}_r - \mathbf{x}\|^2 - \frac{1}{\sigma_s^2} \left\| \mathbf{y}_s - \sum_{k=1}^K \gamma_k \mathcal{D}(\tau_k, f_k) \mathbf{x} \right\|^2 \right\} \quad (14)$$

where

$$\mathbf{C}_{2M} = \begin{bmatrix} \sigma_r^2 \mathbf{I}_M & \mathbf{0}_{M \times M} \\ \mathbf{0}_{M \times M} & \sigma_s^2 \mathbf{I}_M \end{bmatrix}. \quad (15)$$

The log-likelihood function (LLF) can be written as

$$\log p(\mathbf{z}|\boldsymbol{\theta}) = s_1(\mathbf{x}) + s_2(\mathbf{x}, \boldsymbol{\theta}) \quad (16)$$

where

$$s_1(\mathbf{x}) = (P-N) \log \pi - \log \det(\pi\mathbf{C}_{2M}) - \frac{1}{\sigma_r^2} (\mathbf{y}_r - \mathbf{x})^H (\mathbf{y}_r - \mathbf{x}) - \frac{1}{\sigma_s^2} \mathbf{y}_s^H \mathbf{y}_s, \quad (17)$$

$$s_2(\mathbf{x}, \boldsymbol{\theta}) = (P-N) \log \sigma^2 - \frac{1}{\sigma^2} (\mathbf{x}_P^H \mathbf{x}_P + \mathbf{x}_P^H \mathbf{Y}\mathbf{a} + \mathbf{a}^H \mathbf{Y}^H \mathbf{x}_P + \mathbf{a}^H \mathbf{Y}^H \mathbf{Y}\mathbf{a}) - \frac{1}{\sigma_s^2} \sum_{k_1=1}^K \sum_{k_2=1}^K \gamma_{k_1} \gamma_{k_2}^* \mathbf{x}^H \mathcal{D}^H(\tau_{k_2}, f_{k_2}) \mathcal{D}(\tau_{k_1}, f_{k_1}) \mathbf{x} + \frac{2}{\sigma_s^2} \Re \left\{ \sum_{k=1}^K \gamma_k^* \mathbf{x}^H \mathcal{D}^H(\tau_k, f_k) \mathbf{y}_s \right\}. \quad (18)$$

The EM algorithm is an iterative method. Each iteration consists of an expectation step (E-step) and a maximization step (M-step). At the very beginning of the algorithm, it needs an initial guess of the unknown parameters, which is considered in Section III-D.

1) *E-Step*: Taking the expectation of the LLF and dropping $s_1(\mathbf{x})$ in (16), which is independent of θ , we have

$$Q(\theta; \hat{\theta}^{(l)}) \triangleq E_{\mathbf{x}|\mathbf{y}, \hat{\theta}^{(l)}}\{s_2(\mathbf{x}, \theta)\}. \quad (19)$$

We need to compute the expectation of each term in $s_2(\mathbf{x}, \theta)$ to find an explicit expression for $Q(\theta; \hat{\theta}^{(l)})$. Since the vectors \mathbf{x} and \mathbf{y} are jointly Gaussian distributed with zero mean, the posterior mean $\hat{\mathbf{x}}^{(l)} = E_{\mathbf{x}|\mathbf{y}, \hat{\theta}^{(l)}}\{\mathbf{x}\}$ has a closed-form expression [30, p. 324]:

$$\begin{aligned} \hat{\mathbf{x}}^{(l)} &= E\{\mathbf{x}\} + \mathbf{C}_{xy}^{(l)}(\mathbf{C}_{yy}^{(l)})^{-1}(\mathbf{y} - E\{\mathbf{y}\}) \\ &= \mathbf{C}_{xy}^{(l)}(\mathbf{C}_{yy}^{(l)})^{-1}\mathbf{y} \end{aligned} \quad (20)$$

where

$$\begin{aligned} \mathbf{C}_{xy}^{(l)} &= E\{\mathbf{xy}^H; \hat{\theta}^{(l)}\} \\ &= \left[\mathbf{C}_x \left(\hat{\mathbf{a}}^{(l)}, \hat{\sigma}^2{}^{(l)} \right) \quad E\{\mathbf{xy}_s^H; \hat{\theta}^{(l)}\} \right], \end{aligned} \quad (21)$$

$$\begin{aligned} \mathbf{C}_{yy}^{(l)} &= E\{\mathbf{yy}^H; \hat{\theta}^{(l)}\} \\ &= \begin{bmatrix} E\{\mathbf{y}_r \mathbf{y}_r^H; \hat{\theta}^{(l)}\} & E\{\mathbf{y}_r \mathbf{y}_s^H; \hat{\theta}^{(l)}\} \\ E\{\mathbf{y}_s \mathbf{y}_r^H; \hat{\theta}^{(l)}\} & E\{\mathbf{y}_s \mathbf{y}_s^H; \hat{\theta}^{(l)}\} \end{bmatrix}. \end{aligned} \quad (22)$$

The expectation terms in (21) and (22) are given by

$$E\{\mathbf{y}_r \mathbf{y}_r^H; \hat{\theta}^{(l)}\} = \mathbf{C}_x \left(\hat{\mathbf{a}}^{(l)}, \hat{\sigma}^2{}^{(l)} \right) + \sigma_r^2 \mathbf{I}, \quad (23)$$

$$\begin{aligned} E\{\mathbf{y}_r \mathbf{y}_s^H; \hat{\theta}^{(l)}\} &= E\{\mathbf{xy}_s^H; \hat{\theta}^{(l)}\} \\ &= \sum_{k=1}^K \left(\hat{\gamma}_k^{(l)} \right)^* \mathbf{C}_x \left(\hat{\mathbf{a}}^{(l)}, \hat{\sigma}^2{}^{(l)} \right) \mathcal{D}^H \left(\hat{\tau}_k^{(l)}, \hat{f}_k^{(l)} \right), \end{aligned} \quad (24)$$

$$\begin{aligned} E\{\mathbf{y}_s \mathbf{y}_s^H; \hat{\theta}^{(l)}\} &= \sigma_s^2 \mathbf{I} + \sum_{k_1=1}^K \sum_{k_2=1}^K \hat{\gamma}_{k_1}^{(l)} \left(\hat{\gamma}_{k_2}^{(l)} \right)^* \mathcal{D} \left(\hat{\tau}_{k_1}^{(l)}, \hat{f}_{k_1}^{(l)} \right) \\ &\quad \times \mathbf{C}_x \left(\hat{\mathbf{a}}^{(l)}, \hat{\sigma}^2{}^{(l)} \right) \mathcal{D}^H \left(\hat{\tau}_{k_2}^{(l)}, \hat{f}_{k_2}^{(l)} \right). \end{aligned} \quad (25)$$

Also, the posterior correlation matrix is

$$\begin{aligned} \mathbf{R}_{xx|y}^{(l)} &= E_{\mathbf{x}|\mathbf{y}, \hat{\theta}^{(l)}}\{\mathbf{xx}^H\} \\ &= \hat{\mathbf{x}}^{(l)} \left(\hat{\mathbf{x}}^{(l)} \right)^H + E_{\mathbf{x}|\mathbf{y}, \hat{\theta}^{(l)}}\{(\mathbf{x} - \hat{\mathbf{x}}^{(l)})(\mathbf{x} - \hat{\mathbf{x}}^{(l)})^H\} \\ &= \hat{\mathbf{x}}^{(l)} \left(\hat{\mathbf{x}}^{(l)} \right)^H + \mathbf{C}_x \left(\hat{\mathbf{a}}^{(l)}, \hat{\sigma}^2{}^{(l)} \right) \\ &\quad - \mathbf{C}_{xy}^{(l)} (\mathbf{C}_{yy}^{(l)})^{-1} (\mathbf{C}_{xy}^{(l)})^H. \end{aligned} \quad (26)$$

Using the above-mentioned results, we can write (19) as

$$\begin{aligned} Q(\theta; \hat{\theta}^{(l)}) &= (P - N) \log \sigma^2 \\ &\quad - \frac{1}{\sigma^2} \left(c_3^{(l)} + \left(\mathbf{c}_4^{(l)} \right)^H \mathbf{a} + \mathbf{a}^H \mathbf{c}_4^{(l)} + \mathbf{a}^H \mathbf{C}_5^{(l)} \mathbf{a} \right) \\ &\quad - \sum_{k_1=1}^K \sum_{k_2=1}^K \gamma_{k_1} \gamma_{k_2}^* c_1^{(l)}(k_1, k_2) \\ &\quad + 2\Re \left\{ \sum_{k=1}^K \gamma_k^* c_2^{(l)}(k) \right\} \end{aligned} \quad (27)$$

where

$$\begin{aligned} c_1^{(l)}(k_1, k_2) &= E_{\mathbf{x}|\mathbf{y}, \hat{\theta}^{(l)}} \left\{ \frac{1}{\sigma_s^2} \mathbf{x}^H \mathcal{D}^H(\tau_{k_2}, f_{k_2}) \mathcal{D}(\tau_{k_1}, f_{k_1}) \mathbf{x} \right\} \\ &= \frac{1}{\sigma_s^2} \text{tr} \left\{ \mathcal{D}(\tau_{k_1}, f_{k_1}) \mathbf{R}_{xx|y}^{(l)} \mathcal{D}^H(\tau_{k_2}, f_{k_2}) \right\}, \end{aligned} \quad (28)$$

$$\begin{aligned} c_2^{(l)}(k) &= E_{\mathbf{x}|\mathbf{y}, \hat{\theta}^{(l)}} \left\{ \frac{1}{\sigma_s^2} \mathbf{x}^H \mathcal{D}^H(\tau_k, f_k) \mathbf{y}_s \right\} \\ &= \frac{1}{\sigma_s^2} \left(\hat{\mathbf{x}}^{(l)} \right)^H \mathcal{D}^H(\tau_k, f_k) \mathbf{y}_s, \end{aligned} \quad (29)$$

$$c_3^{(l)} = E_{\mathbf{x}|\mathbf{y}, \hat{\theta}^{(l)}} \{ \mathbf{x}_P^H \mathbf{x}_P \} = \sum_{i=P+1}^N [\mathbf{R}_{xx|y}^{(l)}]_{i,i}, \quad (30)$$

$$\begin{aligned} \mathbf{c}_4^{(l)} &= E_{\mathbf{x}|\mathbf{y}, \hat{\theta}^{(l)}} \{ \mathbf{Y}^H \mathbf{x}_P \} \\ &= E_{\mathbf{x}|\mathbf{y}, \hat{\theta}^{(l)}} \{ [\mathbf{x}_P^H \mathbf{x}_{P-1}, \dots, \mathbf{x}_P^H \mathbf{x}_0]^H \} \\ &= \left[\sum_{i=P+1}^N [\mathbf{R}_{xx|y}^{(l)}]_{i-1,i}, \dots, \sum_{i=P+1}^N [\mathbf{R}_{xx|y}^{(l)}]_{i-P,i} \right]^H, \end{aligned} \quad (31)$$

$$\mathbf{C}_5^{(l)} = E_{\mathbf{x}|\mathbf{y}, \hat{\theta}^{(l)}} \{ \mathbf{Y}^H \mathbf{Y} \} \quad (32)$$

with the (p, q) th element given by

$$\left[\mathbf{C}_5^{(l)} \right]_{p,q} = \sum_{i=P+1}^N [\mathbf{R}_{xx|y}^{(l)}]_{i-q, i-p}, \quad p, q = 1, 2, \dots, P. \quad (33)$$

2) *M-Step*: The M-step maximizes the cost function $Q(\theta; \hat{\theta}^{(l)})$ with respect to (w.r.t.) the unknown parameters:

$$\hat{\theta}^{(l+1)} = \arg \max_{\theta} Q(\theta; \hat{\theta}^{(l)}). \quad (34)$$

The maximization is carried out sequentially w.r.t. each group, including the frequencies f , the delays τ , the amplitudes γ , and the AR parameters θ_{AR} . When maximizing w.r.t. a specific group, the other parameters are assumed known using the results from the l th iteration. Note that the cost function (27) is quadratic w.r.t. θ_{AR} and γ , and the closed-form solutions for them can be obtained during each iteration.

For the AR parameters, taking the derivatives w.r.t. \mathbf{a} and σ^2 , respectively, and setting to zeros, we have

$$\hat{\mathbf{a}}^{(l+1)} = - \left(\mathbf{C}_5^{(l)} \right)^{-1} \mathbf{c}_4^{(l)}, \quad (35)$$

$$\hat{\sigma}^2{}^{(l+1)} = \frac{c_3^{(l)} - \left(\mathbf{c}_4^{(l)} \right)^H \left(\mathbf{C}_5^{(l)} \right)^{-1} \mathbf{c}_4^{(l)}}{N - P}. \quad (36)$$

For amplitude estimation, consider the following partial derivatives:

$$\begin{aligned} \frac{\partial Q(\theta; \hat{\theta}^{(l)})}{\partial \gamma_k^*} &= c_2^{(l)}(k) - \sum_{k_1=1}^K \gamma_{k_1} \gamma_{k_1}^* c_1^{(l)}(k_1, k) = 0, \\ & \quad k = 1, \dots, K. \end{aligned} \quad (37)$$

Algorithm 1: EM Estimator.

Input: RC observation \mathbf{y}_r , SC observation \mathbf{y}_s , and convergence tolerance ε .

Output: Estimates of $\hat{\boldsymbol{\theta}} = [\mathbf{f}^T, \boldsymbol{\tau}^T, \boldsymbol{\gamma}^T, \boldsymbol{\theta}_{\text{AR}}^T]^T$.

Let $l = 0$, set the initial value $\hat{\boldsymbol{\theta}}^{(0)}$ as described in Section III-D, and set the covariance matrix of the IO waveform as $\mathbf{C}_x^{(0)} = \mathbf{I}$.

repeat

- 1) E-step: First compute the posterior mean $\hat{\mathbf{x}}^{(l)}$ (20) and the posterior correlation matrix (26). Then use (28)–(31) and (33) to update the cost function.
- 2) M-step:
- 3) Update $\boldsymbol{\gamma}^{(l+1)}$ and $\boldsymbol{\theta}_{\text{AR}}^{(l+1)}$ using (35)–(37).
- 4) Update $\mathbf{f}^{(l+1)}$ and $\boldsymbol{\tau}^{(l+1)}$ using (44) and (54).
- 5) $l = l + 1$;

until $\|\hat{\boldsymbol{\theta}}^{(l+1)} - \hat{\boldsymbol{\theta}}^{(l)}\| < \varepsilon$

return the latest estimate of $\hat{\boldsymbol{\theta}}^{(l+1)}$

The above-mentioned linear equations can be rewritten in matrix form as $\mathbf{A}\hat{\boldsymbol{\gamma}} = \mathbf{b}$, where

$$[\mathbf{A}]_{k_1, k_2} = c_1^{(l)}(k_1, k_2), \quad k_1, k_2 = 1, \dots, K, \quad (38)$$

$$\hat{\boldsymbol{\gamma}} = [\hat{\gamma}_1^{(l+1)}, \dots, \hat{\gamma}_K^{(l+1)}]^T, \quad (39)$$

$$\mathbf{b} = [c_2^{(l)}(1), \dots, c_2^{(l)}(K)]^T. \quad (40)$$

After obtaining the amplitude estimate $\hat{\boldsymbol{\gamma}}^{(l+1)}$, the remaining problem is to estimate the delay and Doppler as

$$\{\hat{\boldsymbol{\tau}}^{(l+1)}, \hat{\mathbf{f}}^{(l+1)}\} = \arg \max_{\boldsymbol{\tau}, \mathbf{f}} Q(\boldsymbol{\tau}, \mathbf{f}; \hat{\boldsymbol{\gamma}}^{(l+1)}, \hat{\boldsymbol{\theta}}_{\text{AR}}^{(l+1)}) \quad (41)$$

where

$$\begin{aligned} Q(\boldsymbol{\tau}, \mathbf{f}; \hat{\boldsymbol{\gamma}}^{(l+1)}, \hat{\boldsymbol{\theta}}_{\text{AR}}^{(l+1)}) &= (P - N) \log \hat{\sigma}_2^{(l+1)} \\ &- \frac{1}{\hat{\sigma}_2^{(l+1)}} \left(c_3^{(l)} + (\mathbf{c}_4^{(l)})^H \hat{\mathbf{a}}^{(l+1)} + (\hat{\mathbf{a}}^{(l+1)})^H \mathbf{c}_4^{(l)} \right. \\ &+ (\hat{\mathbf{a}}^{(l+1)})^H \mathbf{C}_5^{(l)} \hat{\mathbf{a}}^{(l+1)} \left. \right) \\ &- \sum_{k_1=1}^K \sum_{k_2=1}^K \hat{\gamma}_{k_1}^{(l+1)} (\hat{\gamma}_{k_2}^{(l+1)})^* c_1^{(l)}(k_1, k_2) \\ &+ 2\Re \left\{ \sum_{k=1}^K (\hat{\gamma}_k^{(l+1)})^* c_2^{(l)}(k) \right\}. \end{aligned} \quad (42)$$

The above-mentioned maximization may be achieved by a multidimensional search, which is, however, computationally intensive. In the next section, we develop an efficient procedure to solve the problem by utilizing the FFT algorithm and interpolation techniques.

An iteration is complete after all parameters have been updated. The process is repeated until the algorithm converges, e.g., when the following inequality holds for some small tolerance ε : $\|\hat{\boldsymbol{\theta}}^{(l+1)} - \hat{\boldsymbol{\theta}}^{(l)}\| < \varepsilon$. Our proposed estimation algorithm is summarized in Algorithm 1.

C. Fast Implementation

The idea is to first use the FFT to approximately locate the peak of the cost function (42). Then, simple interpolation techniques are applied to interpolate the values of the cost function over the local region with any desired sample spacing, which avoids computing a larger sized FFT and improves the estimation accuracy.

1) *Target Delay and Doppler Estimation:* Consider the estimation of the k_t th target, which has two unknown parameters $\{\tau_{k_t}, f_{k_t}\}$. Neglecting the terms in (42) that are independent of $\{\tau_{k_t}, f_{k_t}\}$, we have

$$\{\hat{\tau}_{k_t}^{(l+1)}, \hat{f}_{k_t}^{(l+1)}\} = \arg \max_{\tau_{k_t}, f_{k_t}} Q_{k_t}(\tau_{k_t}, f_{k_t}) \quad (43)$$

where

$$\begin{aligned} Q_{k_t}(\tau_{k_t}, f_{k_t}) &\triangleq 2\Re \left\{ \left(\hat{\gamma}_{k_t}^{(l+1)} \right)^* c_2^{(l)}(k_t) \right. \\ &\left. - \sum_{k \neq k_t} \hat{\gamma}_k^{(l+1)} (\hat{\gamma}_k^{(l+1)})^* c_1^{(l)}(k, k_t) \right\}. \end{aligned} \quad (44)$$

To estimate the k_t th target, all the other delay and Doppler parameters are fixed to their latest updates.

Both $c_1^{(l)}(k_1, k_2)$ and $c_2^{(l)}(k)$ share the scaling coefficient $\frac{1}{\hat{\sigma}_s^2}$, which can be dropped without affecting the solution.

Therefore, $c_2^{(l)}(k_t)$ can be simplified as

$$\begin{aligned} c_2^{(l)}(k_t) &= (\hat{\mathbf{x}}^{(l)})^H \mathcal{D}^H(\tau_{k_t}, f_{k_t}) \mathbf{y}_s \\ &= (\hat{\mathbf{x}}^{(l)})^H \mathbf{T}^H \mathbf{W}(-\tau_{k_t}, \Delta f)^H \mathbf{T} \mathbf{W}(f_{k_t}, T_s)^H \mathbf{y}_s \\ &= \frac{1}{M} \sum_{p=1}^M \left(\sum_{q=1}^M [\mathbf{G}]_{p,q} e^{-j2\pi(q-1)f_{k_t}T_s} \right) e^{j2\pi(p-1)\tau_{k_t}\Delta f} \end{aligned} \quad (45)$$

where

$$[\mathbf{G}]_{p,q} = \sqrt{M} [\mathbf{x}_f^*]_p [\mathbf{y}_s]_q e^{-j2\pi(p-1)\Delta f(q-1)T_s} \quad (46)$$

and

$$\mathbf{x}_f = \mathbf{T} \hat{\mathbf{x}}^{(l)}. \quad (47)$$

The proof for (45) is provided in Appendix A. According to (46), we can write \mathbf{G} as

$$\mathbf{G} = \mathbf{M} \boldsymbol{\Theta}_x \mathbf{T} \boldsymbol{\Theta}_y \quad (48)$$

where $\boldsymbol{\Theta}_x$ and $\boldsymbol{\Theta}_y$ are diagonal matrices with diagonal elements given by $[\boldsymbol{\Theta}_x]_{m,m} = [\mathbf{x}_f^*]_m$ for $m = 1, \dots, M$ and $[\boldsymbol{\Theta}_y]_{m,m} = [\mathbf{y}_s]_m$ for $m = 1, \dots, M$. \mathbf{T} is the M -point DFT matrix. Note that the last line of (45) is in the form of a two-dimensional (2-D) FFT.

For the second term in (44), we cannot directly apply a 2-D FFT. Instead, we consider the following rank-1 approximation:

$$\begin{aligned} c_1^{(l)}(k, k_t) &= E_{\mathbf{x}|\mathbf{y}, \hat{\boldsymbol{\theta}}^{(l)}} \left\{ \mathbf{x}^H \mathcal{D}^H(\tau_{k_t}, f_{k_t}) \mathcal{D}(\tau_k^{(l)}, f_k^{(l)}) \mathbf{x} \right\} \\ &\approx (\hat{\mathbf{x}}^{(l)})^H \mathbf{T}^H \mathbf{W}(-\tau_{k_t}, \Delta f)^H \mathbf{T} \mathbf{W}(f_{k_t}, T_s)^H \mathcal{D}(\tau_k^{(l)}, f_k^{(l)}) \hat{\mathbf{x}}^{(l)} \\ &= (\hat{\mathbf{x}}^{(l)})^H \mathbf{T}^H \mathbf{W}(-\tau_{k_t}, \Delta f)^H \mathbf{T} \mathbf{W}(f_{k_t}, T_s)^H \hat{\mathbf{x}}^{(l)} \end{aligned} \quad (49)$$

where

$$\bar{\mathbf{x}}^{(l)} = \mathcal{D}(\tau_k^{(l)}, f_k^{(l)})\hat{\mathbf{x}}^{(l)}. \quad (50)$$

Following similar steps used for $c_2^{(l)}(k_t)$, we can write (49) as a 2-D FFT form as in (45), except that the matrix \mathbf{G} is now replaced by

$$\mathbf{G}' = M\mathbf{\Theta}_x\mathbf{T}\mathbf{\Theta}'_y \quad (51)$$

where $\mathbf{\Theta}'_y$ is a diagonal matrix with diagonal elements given by $[\mathbf{\Theta}'_y]_{m,m} = [\bar{\mathbf{x}}]_m$ for $m = 1, \dots, M$.

Thus, the maximization of (43) can be solved by combining the 2-D FFT terms of $c_2^{(l)}(k_t)$ and $c_1^{(l)}(k, k_t)$ in (44) and identifying the peak of the cost function $Q_{k_t}(\tau_{k_t}, f_{k_t})$. Then, the delay and Doppler estimates can be obtained from the peak location $\{u, v\}$ on the 2-D FFT grid through the following relation:

$$\tau_k = -\frac{v-1-M}{\Delta f M}, \quad f_k = \frac{u-1}{T_s M}. \quad (52)$$

2) *Clutter Delay Estimation*: Consider estimating the delay τ_{k_c} of the k_c th clutter component. Dropping the terms in the cost function (42) that are independent of τ_{k_c} , we have

$$\hat{\tau}_{k_c}^{(l+1)} = \arg \max_{\tau_{k_c}} Q_{k_c}(\tau_{k_c}, f_{k_c} = 0) \quad (53)$$

where

$$Q_{k_c}(\tau_{k_c}, f_{k_c} = 0) \triangleq 2\Re \left\{ \hat{\gamma}_{k_c}^{(l+1)*} c_2^{(l)}(k_c) - \sum_{k \neq k_c} \hat{\gamma}_k^{(l+1)} (\hat{\gamma}_{k_c}^{(l+1)})^* c_1^{(l)}(k, k_c) \right\}. \quad (54)$$

For the first term, we have

$$\begin{aligned} c_2^{(l)}(k_c) &= (\hat{\mathbf{x}}^{(l)})^H \mathcal{D}^H(\tau_{k_c}, f_{k_c}) \mathbf{y}_s \\ &= (\hat{\mathbf{x}}^{(l)})^H \mathbf{T}^H \mathbf{W}(-\tau_{k_c} \Delta f)^H \mathbf{T} \mathbf{y}_s \\ &= \mathbf{x}_f^H \mathbf{W}(-\tau_{k_c} \Delta f)^H \mathbf{y}_f \\ &= \frac{1}{M} \sum_{m=1}^M [\mathbf{g}]_m e^{j2\pi(m-1)\tau_{k_c} \Delta f}, \quad f_{k_c} = 0 \end{aligned} \quad (55)$$

where

$$\mathbf{g} = M\mathbf{x}_f^* \odot \mathbf{y}_f, \quad (56)$$

$$\mathbf{x}_f = \mathbf{T}\hat{\mathbf{x}}^{(l)}, \quad \mathbf{y}_f = \mathbf{T}\mathbf{y}_s. \quad (57)$$

It is clear that (55) is an M -point one-dimensional (1-D) inverse FFT (IFFT). For the second term, after a similar rank-1 approximation previously used for target parameter estimation, we have

$$\begin{aligned} c_1^{(l)}(k, k_c) &= E_{\mathbf{x}|\mathbf{y}, \hat{\theta}^{(l)}} \left\{ \mathbf{x}^H \mathcal{D}^H(\tau_{k_c}, f_{k_c}) \mathcal{D}(\tau_k^{(l)}, f_k^{(l)}) \mathbf{x} \right\} \\ &\approx (\hat{\mathbf{x}}^{(l)})^H \mathbf{T}^H \mathbf{W}(-\tau_{k_c} \Delta f)^H \mathbf{T} \mathcal{D}(\tau_k^{(l)}, f_k^{(l)}) \hat{\mathbf{x}}^{(l)}, \quad f_{k_c} = 0. \end{aligned} \quad (58)$$

Following similar steps in (55), we can rewrite (58) as a 1-D IFFT with \mathbf{g} and \mathbf{y}_f replaced by

$$\mathbf{g}' = M\mathbf{x}_f^* \odot \mathbf{y}'_f, \quad (59)$$

$$\mathbf{y}'_f = \mathbf{T}\mathcal{D}(\tau_k^{(l)}, f_k^{(l)}) \hat{\mathbf{x}}^{(l)}. \quad (60)$$

So the delay estimation can be obtained by combining the 1-D IFFT terms of $c_2^{(l)}(k_c)$ and $c_1^{(l)}(k, k_c)$ in (54), and identifying the peak location of the resulting cost function. Finally, the delay estimate can be obtained by the following relationship between the 1-D IFFT grid v and delay τ_k :

$$\tau_k = \frac{v-1}{\Delta f M}. \quad (61)$$

3) *Interpolation*: The above-mentioned fast implementation can find the peak location of the cost function on the FFT or IFFT grid. Further improvement in estimation accuracy can be obtained by interpolating on the FFT or IFFT grid. Here, we consider a simple quadratic 1-D interpolation method using three grid points along either the Doppler or delay dimension. Consider, for example, the interpolation for the clutter delay estimation. Let v_0 denote the peak location of the cost function on the IFFT grid. For notational simplicity, we write the cost function (54) evaluated at the v th IFFT grid as $Q_{k_c}(v)$. The 3-point quadratic interpolation employs $Q_{k_c}(v_0)$ as well as two adjacent IFFT points on both sides of the peak location, i.e., $Q_{k_c}(v_0 - 1)$ and $Q_{k_c}(v_0 + 1)$, and computes an offset of the peak location as [31, pp. 264–270]

$$\Delta v = \frac{-\frac{1}{2} \left\{ |\hat{Q}_{k_c}^{(l+1)}(v_0 + 1)| - |\hat{Q}_{k_c}^{(l+1)}(v_0 - 1)| \right\}}{|\hat{Q}_{k_c}^{(l+1)}(v_0 - 1)| - 2|\hat{Q}_{k_c}^{(l+1)}(v_0)| + |\hat{Q}_{k_c}^{(l+1)}(v_0 + 1)|}. \quad (62)$$

The new peak location following interpolation is then given by $v_0 + \Delta v$. Converting the grid location to delay, we have the following updated delay estimate:

$$\tau_k = \frac{v_0 - 1 + \Delta v}{\Delta f M}. \quad (63)$$

Due to its simple closed form, the above-mentioned interpolation can be applied every time an IFFT peak is identified, i.e., for each EM iteration. Similar interpolation can be applied to improve the target delay and Doppler estimates. Finally, for such FFT- or IFFT-based interpolation methods, it is often recommended to apply a window function prior to taking the FFT or IFFT to ensure the three adjacent points are on the same main lobe of the cost function [31].

D. Parameter Initialization

In this section, we discuss the initialization for the proposed EM algorithm. First, the EM algorithm requires initial estimates of the IO waveform covariance matrix $\mathbf{C}_x(\mathbf{a}, \sigma^2)$, which depends on the AR parameters. Here, we initialize it as an identity matrix, which means that the waveform correlation is ignored for the initialization. Next, the amplitudes, delays, and Doppler frequencies are initialized through the following process, henceforth referred

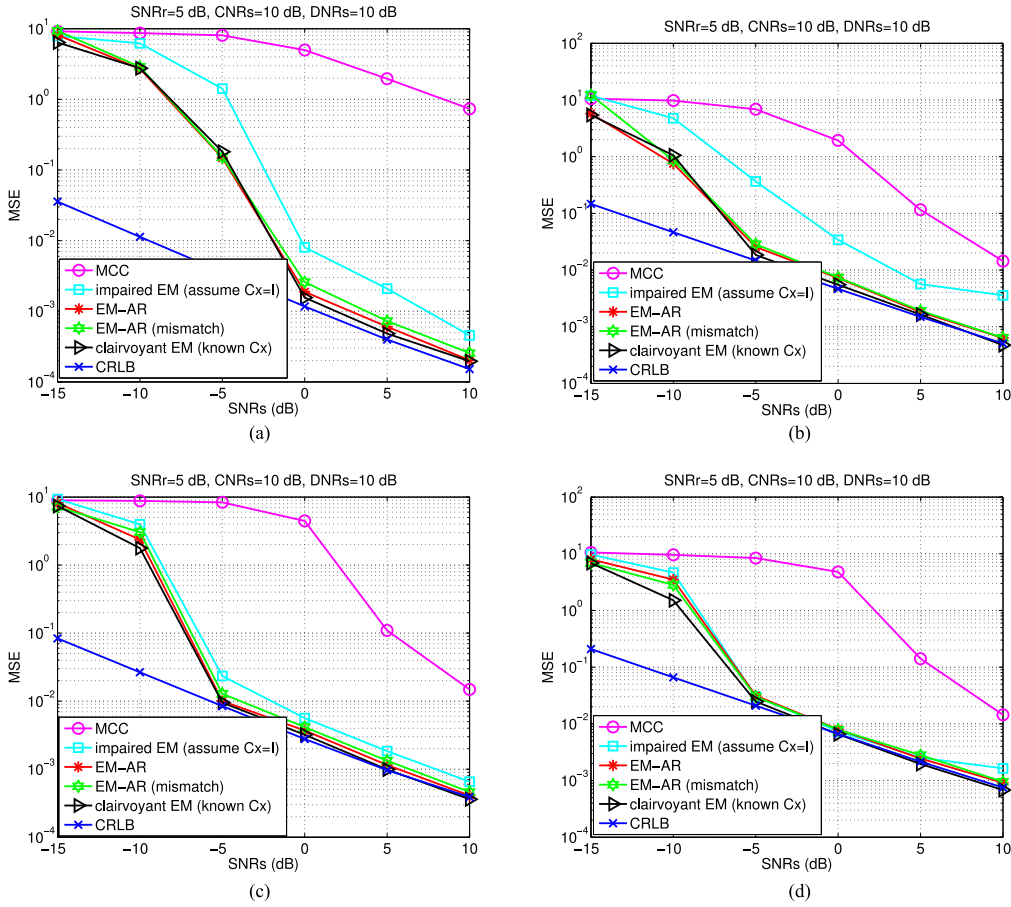


Fig. 2. MSE versus SNR, with highly ($\rho = 0.9$) and lowly ($\rho = 0.1$) correlated IO waveforms. (a) Target delay and (b) target Doppler with $\rho = 0.9$; and (c) target delay and (d) target Doppler with $\rho = 0.1$.

to as the MCC estimator, since it is able to obtain coarse estimates of these parameters. The MCC is based on the widely used *successive interference cancellation* method, which starts with sequentially estimating and canceling the stronger signal components (e.g., DPI and clutter) from the observed signal, and then using the residual to estimate the weaker signal components (e.g., target signals). In the following, we briefly summarize the main steps of the MCC. For simplicity, we assume there is only one clutter dominant scatterer and one target component in the observation. The extension to the case with multicomponents for each signal category is straightforward.

By ignoring the presence of the target and clutter, a coarse estimate of the DPI amplitude can be obtained by least-squares (LS):

$$\bar{\gamma}_1 = \frac{\mathbf{y}_r^H \mathbf{y}_s}{\|\mathbf{y}_r\|^2}. \quad (64)$$

Using the reference signal \mathbf{y}_r as an estimate of the IO waveform, we can cancel the DPI in \mathbf{y}_s :

$$\mathbf{y}'_1 = \mathbf{y}_s - \bar{\gamma}_1 \mathbf{y}_r. \quad (65)$$

The DPI-canceled signal can be used for clutter delay estimation (ignoring the presence of the target signal):

$$\bar{\tau}_3 = \arg \max_{\tau} |\mathbf{y}'_1{}^H \mathbf{T}^H \mathbf{W}(-\tau \Delta f) \mathbf{T} \mathbf{y}_r|. \quad (66)$$

The clutter signal amplitude can be obtained by LS:

$$\bar{\gamma}_3 = \frac{(\mathbf{T}^H \mathbf{W}(-\bar{\tau}_3 \Delta f) \mathbf{T} \mathbf{y}_r)^H \mathbf{y}'_1}{\|\mathbf{T}^H \mathbf{W}(-\bar{\tau}_3 \Delta f) \mathbf{T} \mathbf{y}_r\|^2}. \quad (67)$$

Then, we can cancel the clutter component:

$$\mathbf{y}'_2 = \mathbf{y}'_1 - \bar{\gamma}_3 \mathbf{T}^H \mathbf{W}(-\bar{\tau}_3 \Delta f) \mathbf{T} \mathbf{y}_r. \quad (68)$$

The residual is next used for target delay and Doppler estimation:

$$\{\bar{\tau}_2, \bar{f}_2\} = \arg \max_{\tau, f} |\mathbf{y}'_2{}^H \mathbf{W}(f T_s) \mathbf{T}^H \mathbf{W}(-\tau \Delta f) \mathbf{T} \mathbf{y}_r|. \quad (69)$$

Finally, the target echo amplitude is obtained by LS:

$$\bar{\gamma}_2 = \frac{(\mathbf{W}(\bar{f}_2 T_s) \mathbf{T}^H \mathbf{W}(-\bar{\tau}_2 \Delta f) \mathbf{T} \mathbf{y}_r)^H \mathbf{y}'_2}{\|\mathbf{W}(\bar{f}_2 T_s) \mathbf{T}^H \mathbf{W}(-\bar{\tau}_2 \Delta f) \mathbf{T} \mathbf{y}_r\|^2}. \quad (70)$$

E. Cramér–Rao Lower Bound

The unknown parameters in the estimation problem include

$$\boldsymbol{\phi} = \left[\underbrace{\mathbf{f}^T}_{1 \times K_r}, \underbrace{\boldsymbol{\tau}^T}_{1 \times (K_r + K_c)}, \underbrace{\boldsymbol{\phi}_Y^T}_{1 \times 2K}, \underbrace{\boldsymbol{\phi}_{AR}^T}_{1 \times (2P+1)} \right]^T \quad (71)$$

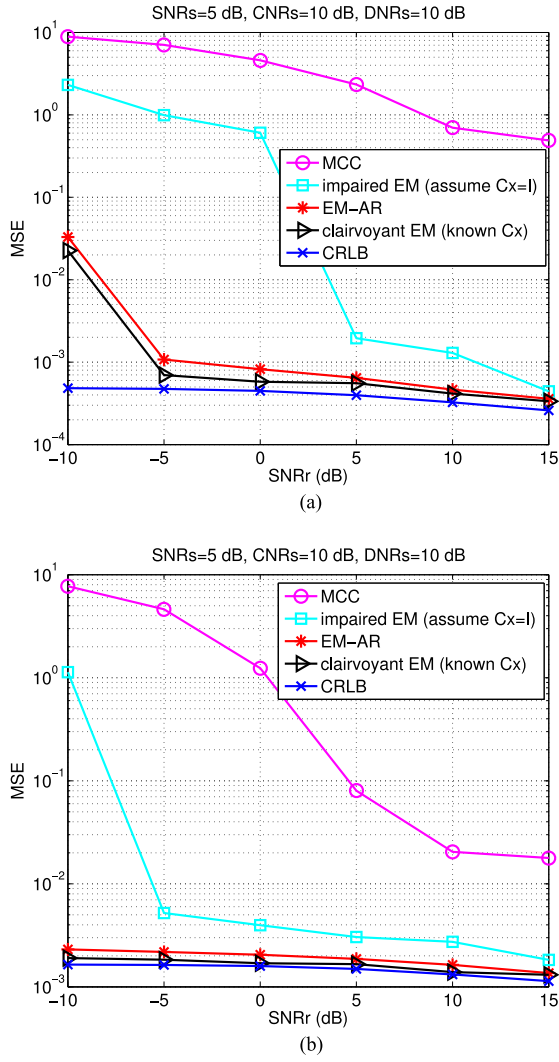


Fig. 3. MSE versus SNR_r when $\rho = 0.9$. (a) Target delay and (b) target Doppler.

where $K = K_t + K_c + 1$, $\mathbf{f} = [f_2, \dots, f_{K_t+1}]^T$, $\boldsymbol{\tau} = [\tau_2, \dots, \tau_K]^T$, $\boldsymbol{\phi}_\gamma = [\gamma_1^r, \dots, \gamma_K^r, \gamma_1^i, \dots, \gamma_K^i]^T$ are the real and imaginary parts of the complex amplitudes, and $\boldsymbol{\phi}_{\text{AR}} = [\Re\{\mathbf{a}^T\}, \Im\{\mathbf{a}^T\}, \sigma^2]^T$ are AR parameters. The total number of unknown parameters is $L = 4K_t + 3K_c + 2P + 3$.

By the Slepian–Bangs formula, the entries of the $L \times L$ Fisher information matrix (FIM) \mathbf{F} are given by [30, pp. 524–525]

$$[\mathbf{F}]_{i,j} = \text{tr} \left\{ \mathbf{C}_y^{-1}(\boldsymbol{\phi}) \frac{\partial \mathbf{C}_y(\boldsymbol{\phi})}{\partial \theta_i} \mathbf{C}_y^{-1}(\boldsymbol{\phi}) \frac{\partial \mathbf{C}_y(\boldsymbol{\phi})}{\partial \theta_j} \right\}, \quad i, j = 1, \dots, L \quad (72)$$

where $\mathbf{C}_y(\boldsymbol{\phi})$ has the same form as $\mathbf{C}_{yy}^{(l)}$ in (22) except that the unknown parameters are $\boldsymbol{\phi}$ instead of the estimate $\hat{\boldsymbol{\theta}}^{(l)}$.

Details of computing the partial derivatives used in the FIM are provided in Appendix B. The CRLB is given by the diagonal elements of the inverse of the FIM:

$$\text{CRLB}([\boldsymbol{\phi}]_l) = [\mathbf{F}^{-1}]_{l,l}, \quad l = 1, \dots, L. \quad (73)$$

IV. NUMERICAL SIMULATIONS

In this section, numerical simulations are provided to demonstrate the performance of the proposed estimators in DPI and clutter-contaminated environment. In the simulations, we first consider two types of simulated IO waveforms and then examine the performance of the various estimators using FM signals.

The first type of simulated IO waveforms is first-order AR processes with the AR coefficient a and driving noise variance σ^2 , which are used to compute the ACF sequence using the Yule–Walker equations. The temporal covariance matrix is Hermitian, Toeplitz, and is fully determined by the ACF sequence. The second type of simulated IO waveforms reflects a more practical scenario, where each IO waveform is generated as a correlated stochastic process that has a widely used Gaussian-shaped power spectral density (PSD) but is not an AR process. Specifically, the temporal correlation of the random process denoted by

the correlation lag n is given by $r(n) = P_x e^{-\frac{n^2}{2\delta_v^2}}$, where P_x denotes the average power of the waveform and δ_v is the standard deviation that specifies how rapidly the waveform fluctuates in time: a small value of δ_v implies that the waveform is lowly correlated and vice versa. The IO waveform covariance matrix \mathbf{C}_x as a function of δ_v is obtained from the above-mentioned temporal correlation: $r(0), r(1), \dots, r(N-1)$. It should be noted that with the Gaussian-shaped PSD, the random process is not an AR process. In this case, there is a *model mismatch* with our proposed AR model based EM estimator. Nevertheless, as we shall see, even with mismatch, the AR process is still able to effectively capture the temporal correlation of the random waveform, which allows us to exploit the correlation for passive sensing. Under both data models, the correlation is measured by the following correlation parameter:

$$\rho = \frac{1}{N-1} \sum_{n=0}^{N-2} \left| \frac{r(n+1)}{r(n)} \right|. \quad (74)$$

In the sequel, we will test different estimators under both *high correlation* and *low correlation* scenarios measured by ρ .

We assume that the noise in the RC and SC is zero-mean white Gaussian with variance σ_s^2 and σ_r^2 , respectively. The SNR in the RC is defined as

$$\text{SNR}_r = \frac{N P_x}{M \sigma_r^2} \quad (75)$$

where M is the observation length, while N is the length of the IO waveform. $P_x = \frac{\sigma^2}{1-|a|^2}$ is the average power of the IO waveform. The DPI-to-noise ratio (DNR) in the SC is

$$\text{DNR}_s = \frac{N P_x |\gamma_l|^2}{M \sigma_s^2} \quad (76)$$

the SNR in the SC is

$$\text{SNR}_s = \frac{N P_x |\gamma_l|^2}{M \sigma_s^2} \quad (77)$$

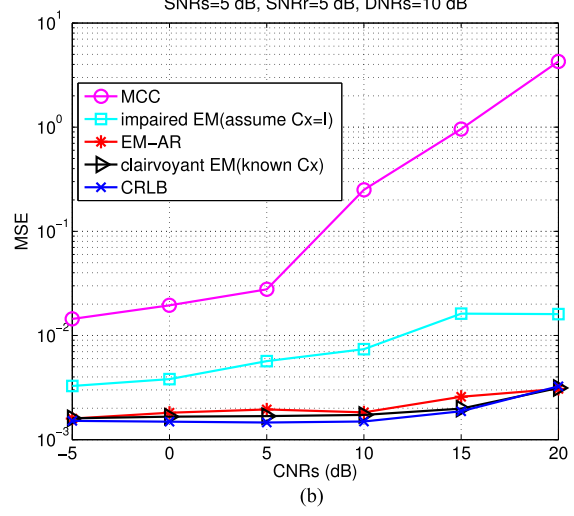
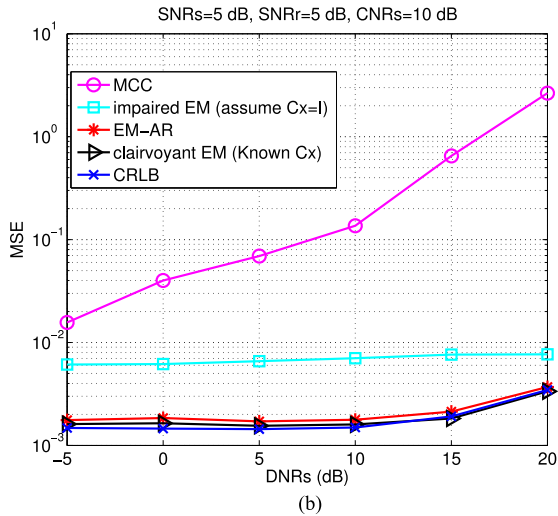
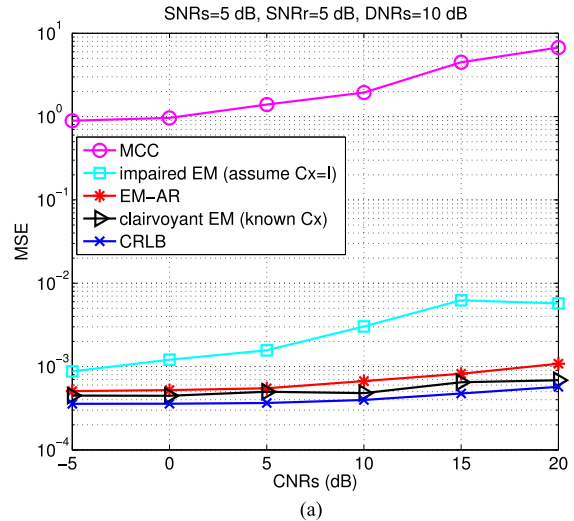
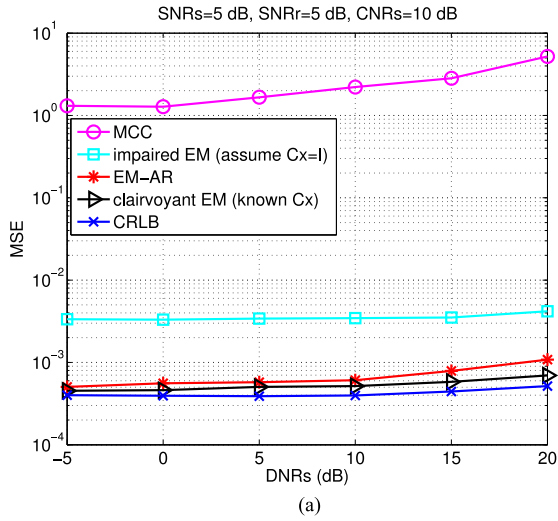


Fig. 4. MSE versus DNR_s when $\rho = 0.9$. (a) Target delay and (b) target Doppler.

Fig. 5. MSE of the estimator under different CNR_s when $\rho = 0.9$. (a) Target delay and (b) target Doppler.

and the clutter-to-noise ratio (CNR) in the SC is

$$CNR_s = \frac{N P_x |\gamma_c|^2}{M \sigma_s^2} \quad (78)$$

where γ_t is the target echo amplitude and γ_c is the clutter echo amplitude.

The following methods are considered in our simulations. We consider several EM-based estimators with variations. The first is our proposed AR model based EM, denoted as *EM-AR*. The second is an *impaired EM*, which ignores the IO waveform correlation by setting the waveform covariance matrix $\mathbf{C}_x = \mathbf{I}$. The third is a *clairvoyant EM*, which assumes \mathbf{C}_x is known and bypasses the related estimation. Clearly, the clairvoyant EM offers a benchmark for the proposed EM-AR estimator. Also included in comparison is the successive interference cancellation based *MCC* method (see Section III-D), which offers coarse estimates of the parameters but is computationally efficient. The above-mentioned estimators are tested with simulated data generated by using the first kind IO waveform, i.e., AR model based waveform, for

which case the CRLB can be evaluated and is included for comparison. Finally, our EM-AR estimator is also tested with the second kind IO (non-AR) waveforms, and the corresponding results are shown under *EM-AR (mismatch)* to illustrate how model mismatch affects the performance of the EM-AR estimator. Since the other estimators do not impose the AR assumption, their results, in this case, are unaffected and thus omitted due to space limitation.

The simulated data include one target signal, DPI, and one major clutter component with the following parameters unless otherwise stated: target Doppler $f_t = \frac{25.12 f_s}{M}$ Hz, target delay $\tau_t = 28.89 T_s$, and clutter delay $\tau_c = 10.24 T_s$, where f_s is the sampling rate in Hz, T_s is the sampling interval in seconds, and M is the number of samples in time and also the number of samples in frequency when converting the signal to the frequency domain [cf., (5)]. The IO waveforms are randomly generated from trial to trial. For the first type of IO waveform, the AR driving noise variance $\sigma^2 = 10$. We set the FFT size $N_c = 1024$, the observation length $M = 100$, and IO waveform duration $N = 70$.

Fig. 2 shows the mean squared error (MSE) for the target delay and Doppler under both high correlation and low

correlation scenarios with different SNR_s when $\text{DNR}_s = 10$ dB, $\text{CNR}_s = 10$ dB, and $\text{SNR}_r = 5$ dB. In Fig. 2(a) and 2(b), where $\rho = 0.9$, the results show that the MSE of the clairvoyant EM reaches the CRLB at high SNR_s , and the performance of the EM-AR is very close to that of the clairvoyant EM. It is also seen that the impaired EM is notably worse than the EM-AR since the former does not exploit the waveform correlation. The EM-AR with mismatch experiences a slight degradation but is still better than the impaired EM. Despite its computational efficiency, the MCC estimator has the worst performance. In Fig. 2(c) and (d), where $\rho = 0.1$, the MSE curves have a similar trend except that the performance of the impaired EM gets closer to that of the EM-AR, comparing to the former higher correlation case. This is expected since with low correlation implies less benefit can be derived from exploiting the correlation.

The estimation performance versus SNR_r is shown in Fig. 3, where $\rho = 0.9$, $\text{DNR}_s = 10$ dB, $\text{CNR}_s = 10$ dB, and $\text{SNR}_s = 5$ dB. It is observed that all the methods seem to benefit from a better RC measured by a higher SNR_r . It can be seen that the performance gap between the proposed EM-AR and the clairvoyant EM is very small and both approach the CRLB, while the impaired EM is much worse than its two counterparts and only approaches the latter at very high SNR_r . It can also be seen that the MCC fails to accurately estimate the target delay, although it has better Doppler estimate at high SNR_r .

In Fig. 4, the estimation performance is presented as a function of DNR_s , where $\rho = 0.9$, $\text{CNR}_s = 10$ dB, $\text{SNR}_r = 5$ dB, and $\text{SNR}_s = 5$ dB. We can see that increasing DNR_s does not lead to significant performance difference for the three EM estimators, while the MCC is more sensitive to the DPI. The proposed EM-AR is again very close to the clairvoyant EM, indicating the effectiveness of the AR model in exploiting the waveform correlation to enhance estimation accuracy.

Fig. 5 shows the estimation performance versus CNR_s , where $\rho = 0.9$, $\text{DNR}_s = 10$ dB, $\text{SNR}_r = 5$ dB, and $\text{SNR}_s = 5$ dB. In this scenario, it can be seen that there is some degradation for target estimation as the clutter gets stronger with increasing CNR_s . The performance of the proposed EM-AR is very similar to that of the clairvoyant EM. Both outperform the impaired EM. The MCC is much worse than the other estimators and exhibits substantial performance degradation as CNR_s increase.

Fig. 6 shows a scenario where two targets and two clutter scatterers are included in the simulation data. The parameters associated with the first target and the first clutter scatterer are the same, as shown in Fig. 4. The parameters associated with the second target are $f_t = \frac{29.06 f_s}{M}$ Hz, $\tau_t = 20.94 T_s$ s, and $\text{SNR}_s = 5$ dB. The parameters associated with the second clutter scatterer are $\tau_c = 16.19 T_s$ s and $\text{CNR}_s = 5$ dB. For the proposed EM-AR estimator, the MSE of delay and Doppler of the first target is similar, as shown in Fig. 4. Fig. 6 depicts the performance of the various estimators and CRLB for the second target. The results show that while the heuristic MCC experiences notable degradation,

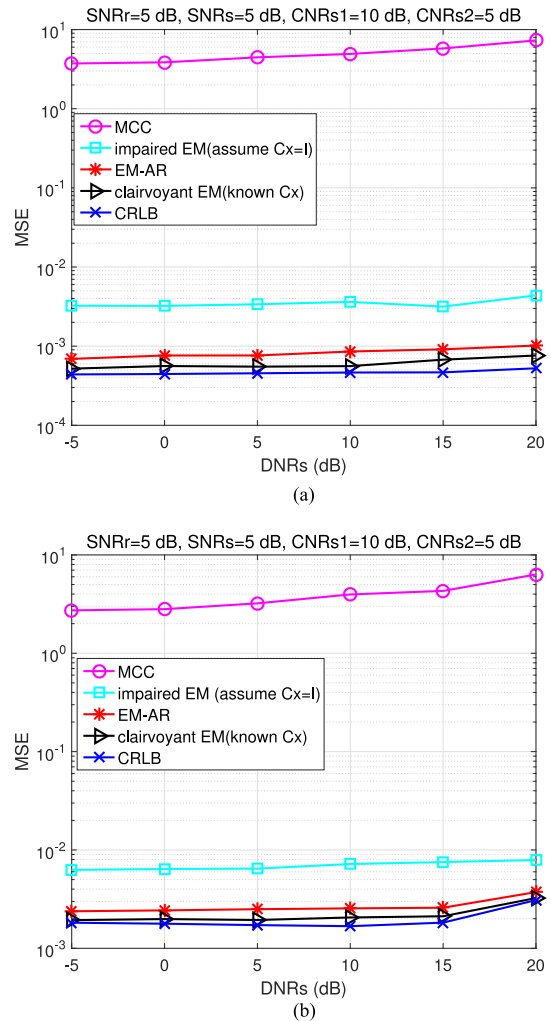


Fig. 6. MSE of the estimator under different DNR_s with two targets and two clutterers. (a) Target2 delay and (b) target2 Doppler.

the proposed EM-AR is still close to the CRLB for the multitarget, multiclutter-scatterer scenario.

Finally, we test the performance of the various estimators by using FM signals, which are widely considered for passive radar applications [11]–[13], [32], [33]. The estimation performance of using an FM waveform as the IO signal versus SNR_s is shown in Fig. 7, where $\text{DNR}_s = 10$ dB, $\text{CNR}_s = 10$ dB, and $\text{SNR}_r = 5$ dB. Because the exact covariance matrix of the FM radio signal is unknown, the clairvoyant EM cannot be implemented and is skipped in this simulation. The results show that the proposed EM-AR still outperforms the impaired EM with a similar performance gain when compared with the results in Fig. 2(a) and (b) that were based on simulated IO waveforms.

V. CONCLUSION

In this paper, we have addressed the parameter estimation problem for passive radar by exploiting the correlation of the IO waveform. We proposed an EM-AR approach in the presence of noise, DPI, and clutter by modeling the waveform as an AR process. The AR model is then integrated into an EM framework for parameter estimation.

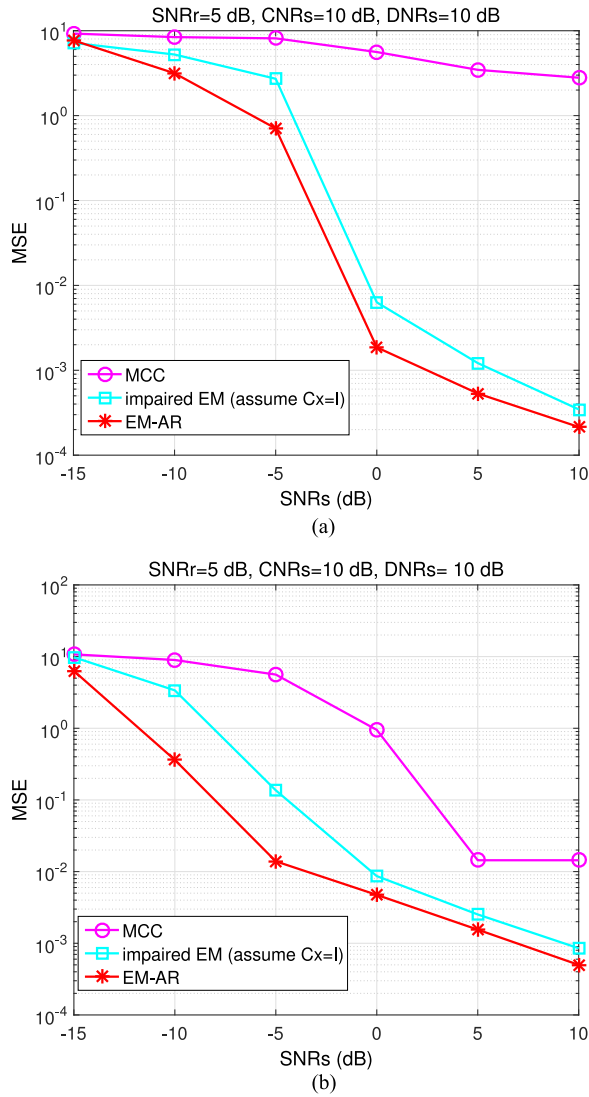


Fig. 7. MSE of the estimator under different SNR_s using FM waveform as IO signal. (a) Target delay and (b) target Doppler.

We also proposed a fast implementation scheme based on the FFT and interpolation to replace the conventional 1-D and 2-D search commonly used in the EM algorithm. The performance assessment, which has been undertaken under various scenarios, has shown that the proposed EM-AR estimator is close to the clairvoyant EM, which assumes knowledge of the waveform covariance matrix. Both are close to the CRLB under a wide range of operation conditions. Both also greatly outperform the impaired EM that ignores the waveform correlation. Our results indicate that using the AR model to exploit the correlation of the IO waveform is an effective way to enhance passive sensing performance.

APPENDIX

A. Proof of (45)

The proof proceeds by calculation. Using the definition in (47), we have

$$\begin{aligned} c_2^{(l)}(k_t) &= (\hat{\mathbf{x}}^{(l)})^H \mathbf{T}^H \mathbf{W}(-\tau_{k_t} \Delta f)^H \mathbf{T} \mathbf{W}(f_{k_t} T_s)^H \mathbf{y}_s \\ &= (\mathbf{T} \hat{\mathbf{x}}^{(l)})^H \mathbf{W}(-\tau_{k_t} \Delta f)^H (\mathbf{T} \mathbf{W}(f_{k_t} T_s)^H \mathbf{y}_s) \\ &= \sum_{p=1}^M [\mathbf{g}]_p e^{j2\pi(p-1)\tau_{k_t} \Delta f} \end{aligned} \quad (79)$$

where $\mathbf{g} \triangleq \mathbf{x}_f^* \odot \mathbf{h}$, and $\mathbf{h} \triangleq \mathbf{T} \mathbf{W}(f_{k_t} T_s)^H \mathbf{y}_s$. Since $[\mathbf{T}]_{p,q} = \frac{1}{\sqrt{M}} e^{-j2\pi(p-1)\Delta f(q-1)T_s}$ and $[\mathbf{W}(x)]_{p,p} = e^{j2\pi(p-1)x}$, we have

$$[\mathbf{h}]_p = \frac{1}{\sqrt{M}} \sum_{q=1}^M [\mathbf{y}_s]_q e^{-j2\pi(q-1)f_{k_t} T_s} e^{-j2\pi(p-1)\Delta f(q-1)T_s}. \quad (80)$$

Then, we have

$$\begin{aligned} [\mathbf{g}]_p &= \frac{[\mathbf{x}_f^*]_p}{\sqrt{M}} \sum_{q=1}^M [\mathbf{y}_s]_q e^{-j2\pi(q-1)f_{k_t} T_s} e^{-j2\pi(p-1)\Delta f(q-1)T_s} \\ &= \frac{1}{M} \sum_{q=1}^M [\mathbf{G}]_{p,q} e^{-j2\pi(q-1)f_{k_t} T_s} \end{aligned} \quad (81)$$

where

$$[\mathbf{G}]_{p,q} = \sqrt{M} [\mathbf{x}_f^*]_p [\mathbf{y}_s]_q e^{-j2\pi(p-1)\Delta f(q-1)T_s}. \quad (82)$$

Hence, (79) can be rewritten as

$$\begin{aligned} c_2^{(l)}(k_t) &= \sum_{p=1}^M [\mathbf{g}]_p e^{j2\pi(p-1)\tau_{k_t} \Delta f} \\ &= \frac{1}{M} \sum_{p=1}^M \left[\sum_{q=1}^M [\mathbf{G}]_{p,q} e^{-j2\pi(q-1)f_{k_t} T_s} \right] e^{j2\pi(p-1)\tau_{k_t} \Delta f}. \end{aligned} \quad (83)$$

B. Fisher Information Matrix

Recall the parameter set defined in (71), repeated as follows for easy reference:

$$\boldsymbol{\phi} = \left[\underbrace{\mathbf{f}^T}_{1 \times K_t}, \underbrace{\boldsymbol{\tau}^T}_{1 \times (K_t + K_c)}, \underbrace{\boldsymbol{\phi}_\gamma^T}_{1 \times 2K}, \underbrace{\boldsymbol{\phi}_{\text{AR}}^T}_{1 \times (2P+1)} \right]^T.$$

The FIM (72) involves computing the partial derivative of $\mathbf{C}_y(\boldsymbol{\phi})$ w.r.t. the individual group of parameters. To simplify the notation in the following derivation, we define $\mathbf{E} \triangleq E\{\mathbf{y}_r \mathbf{y}_r^H; \boldsymbol{\phi}\}$, $\mathbf{H} \triangleq E\{\mathbf{y}_r \mathbf{y}_r^H; \boldsymbol{\phi}\}$, and $\mathbf{J} \triangleq E\{\mathbf{y}_s \mathbf{y}_s^H; \boldsymbol{\phi}\}$ to represent the composing block matrices of $\mathbf{C}_y(\boldsymbol{\phi})$, similar to those in (22).

First consider the partial derivatives of \mathbf{E} , which only depends on the AR parameters. Therefore, the partial derivatives of \mathbf{E} w.r.t. \mathbf{f} , $\boldsymbol{\tau}$, and $\boldsymbol{\phi}_\gamma$ are zeros, i.e.,

$$\frac{\partial \mathbf{E}}{\partial [\boldsymbol{\phi}]_\ell} = 0, \quad \ell = 1, \dots, L - 2P - 1 \quad (84)$$

and the partial derivatives of \mathbf{E} w.r.t. $\boldsymbol{\phi}_{\text{AR}}$ are

$$\frac{\partial \mathbf{E}}{\partial [\boldsymbol{\phi}]_\ell} = \boldsymbol{\Psi}_\ell, \quad \ell = L - 2P, \dots, L \quad (85)$$

where the specific form of Ψ_ℓ depends on the IO waveform covariance matrix $\mathbf{C}_x(\mathbf{a}, \sigma^2)$. Note that no closed-form expression for $\mathbf{C}_x(\mathbf{a}, \sigma^2)$ for a general AR model exists. However, it can be recursively determined by the inverse Levinson algorithm from \mathbf{a} and σ^2 [28]. Consider, e.g., the first-order AR process. The covariance matrix is given by

$$[\mathbf{C}_x(a, \sigma^2)]_{m,n} = \frac{\sigma^2(-a)^{|m-n|}}{1 - |a|^2}, \quad m, n = 1, \dots, N, \quad (86)$$

In this case, we have $P = 1$, and it is easy to show that the $M \times M$ matrix Ψ_ℓ for $\ell = L - 2, \dots, L$ is given by

$$\begin{aligned} [\Psi_{L-2}]_{m,n} &= \frac{|m-n|(|a|^2 - 1) - 2a\Re\{a\}}{(1 - |a|^2)^2(-a)^{1-|m-n|}} \sigma^2, \\ [\Psi_{L-1}]_{m,n} &= \frac{|m-n|(|a|^2 - 1) - 2a\Im\{a\}}{(1 - |a|^2)^2(-a)^{1-|m-n|}} \sigma^2, \\ [\Psi_L]_{m,n} &= \frac{(-a)^{|m-n|}}{1 - |a|^2}, \quad m, n = 1, \dots, N. \end{aligned} \quad (87)$$

For notational simplicity, we use the following shorthand notation for the delay-Doppler shifting matrix [cf., (5)]:

$$\mathcal{D}_k \triangleq \mathcal{D}(\tau_k, f_k). \quad (88)$$

Now, we consider the partial derivatives of \mathbf{H} . The partial derivatives of \mathbf{H} w.r.t. the target Doppler f , i.e., $[\phi]_\ell$ for $\ell = 1, \dots, K_t$, can be expressed as

$$\frac{\partial \mathbf{H}}{\partial [\phi]_\ell} = \gamma_{\ell+1}^* \mathbf{C}_x \mathcal{D}_{\ell+1}^H \Lambda_f^H \quad (89)$$

where Λ_f is a diagonal matrix with diagonal elements $[\Lambda_f]_{m,m} = j2\pi m T_s$, $m = 1, \dots, M$. The partial derivatives of \mathbf{H} w.r.t. the target and clutter delay τ , i.e., $[\phi]_\ell$ for $\ell = K_t + 1, \dots, 2K_t + K_c$, are given by

$$\frac{\partial \mathbf{H}}{\partial [\phi]_\ell} = \gamma_{\ell-K_t+1}^* \mathbf{C}_x \mathcal{D}_{\ell-K_t+1}^H \Lambda_t^H \quad (90)$$

where Λ_t is diagonal with diagonal elements $[\Lambda_t]_{m,m} = -j2\pi m \Delta f$, for $m = 1, \dots, M$. The partial derivatives of \mathbf{H} w.r.t. the real parts of the complex amplitude, i.e., $[\phi]_\ell$ for $\ell = 2K_t + K_c + 1, \dots, 2K_t + K_c + K$, are

$$\frac{\partial \mathbf{H}}{\partial [\phi]_\ell} = \mathbf{C}_x \mathcal{D}_{\ell-2K_t-K_c}^H \quad (91)$$

and the partial derivatives of \mathbf{H} w.r.t. the imaginary parts of the complex amplitude, i.e., $[\phi]_\ell$ for $\ell = 2K_t + K_c + K + 1, \dots, 2K_t + K_c + 2K$, are

$$\frac{\partial \mathbf{H}}{\partial [\phi]_\ell} = -j \frac{\partial \mathbf{H}}{\partial [\phi]_{\ell-K}}. \quad (92)$$

The partial derivatives of \mathbf{H} w.r.t. the AR parameters ϕ_{AR} are

$$\frac{\partial \mathbf{H}}{\partial [\phi]_\ell} = \Psi_\ell \sum_{k=1}^K \gamma_k^* \mathcal{D}^H(\tau_k, f_k), \quad \ell = L - 2, \dots, L. \quad (93)$$

Finally, consider the partial derivatives of \mathbf{J} . The partial derivatives of \mathbf{J} w.r.t. the target Doppler f , i.e., $[\phi]_\ell$ for

$\ell = 1, \dots, K_t$, are

$$\begin{aligned} \frac{\partial \mathbf{J}}{\partial [\phi]_\ell} &= \sum_{k=1}^K \gamma_k \gamma_{\ell+1}^* \mathcal{D}_k \mathbf{C}_x \mathcal{D}_{\ell+1}^H \Lambda_f^H \\ &+ \sum_{k=1}^K \gamma_k^* \gamma_{\ell+1} \Lambda_f \mathcal{D}_{\ell+1} \mathbf{C}_x \mathcal{D}_k^H \end{aligned} \quad (94)$$

and the partial derivatives of \mathbf{J} w.r.t. the target and clutter delay τ , i.e., $[\phi]_\ell$ for $\ell = K_t + 1, \dots, 2K_t + K_c$, are

$$\begin{aligned} \frac{\partial \mathbf{J}}{\partial [\phi]_\ell} &= \sum_{k=1}^K \gamma_k \gamma_{\ell-K_t+1}^* \mathcal{D}_k \mathbf{C}_x \mathcal{D}_{\ell-K_t+1}^H \Lambda_t^H \\ &+ \sum_{k=1}^K \gamma_k^* \gamma_{\ell-K_t+1} \Lambda_t \mathcal{D}_{\ell-K_t+1} \mathbf{C}_x \mathcal{D}_k^H. \end{aligned} \quad (95)$$

By defining

$$\Upsilon_i \triangleq \sum_{k=1}^K \gamma_k \mathcal{D}_k \mathbf{C}_x \mathcal{D}_i^H \quad (96)$$

the partial derivatives of \mathbf{J} w.r.t. the real parts of the complex amplitude, i.e., $[\phi]_\ell$ for $\ell = 2K_t + K_c + 1, \dots, 2K_t + K_c + K$, can be expressed as

$$\frac{\partial \mathbf{J}}{\partial [\phi]_\ell} = \Upsilon_{\ell-2K_t-K_c}^H + \Upsilon_{\ell-2K_t-K_c} \quad (97)$$

and the partial derivatives of \mathbf{J} w.r.t. the imaginary parts of the complex amplitude, i.e., $[\phi]_\ell$ for $\ell = 2K_t + K_c + K + 1, \dots, 2K_t + K_c + 2K$, are

$$\frac{\partial \mathbf{J}}{\partial [\phi]_\ell} = j \Upsilon_{\ell-2K_t-K_c-K}^H - j \Upsilon_{\ell-2K_t-K_c-K}. \quad (98)$$

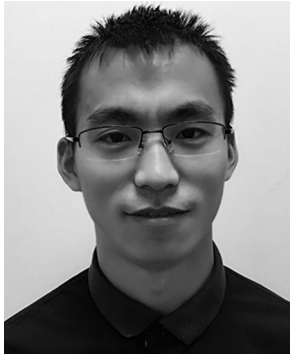
The partial derivatives of \mathbf{J} w.r.t. the AR parameters ϕ_{AR} are

$$\begin{aligned} \frac{\partial \mathbf{J}}{\partial [\phi]_\ell} &= \sum_{k2=1}^K \sum_{k1=1}^K \gamma_{k1} \gamma_{k2}^* \mathcal{D}(\tau_{k1}, f_{k1}) \Psi_\ell \mathcal{D}^H(\tau_{k2}, f_{k2}), \\ \ell &= L - 2, \dots, L. \end{aligned} \quad (99)$$

REFERENCES

- [1] J. E. Palmer, H. A. Harms, S. J. Searle, and L. M. Davis, "DVB-T passive radar signal processing," *IEEE Trans. Signal Process.*, vol. 61, no. 8, pp. 2116–2126, Apr. 2013.
- [2] H. Sun, D. K. P. Tan, Y. Lu, and M. Lesturgie, "Applications of passive surveillance radar system using cell phone base station illuminators," *IEEE Aerosp. Electron. Syst. Mag.*, vol. 25, no. 3, pp. 10–18, Mar. 2010.
- [3] L. Wang and B. Yazici, "Passive imaging of moving targets using sparse distributed apertures," *SIAM J. Imaging Sci.*, vol. 5, no. 3, pp. 769–808, 2012.
- [4] M. Edrich, A. Schroeder, and F. Meyer, "Design and performance evaluation of a mature FM/DAB/DVB-T multi-illuminator passive radar system," *IET Radar, Sonar Navig.*, vol. 8, no. 2, pp. 114–122, Feb. 2014.

- [5] M. Conti, F. Berizzi, E. Dalle Mese, and A. Capria
High range resolution multichannel DVB-T passive radar
IEEE Aerosp. Electron. Syst. Mag., vol. 27, no. 10, pp. 37–42, Oct. 2012.
- [6] S. Gogineni, M. Rangaswamy, B. D. Rigling, and A. Nehorai
Ambiguity function analysis for UMTS-based passive multi-static radar
IEEE Trans. Signal Process., vol. 62, no. 11, pp. 2945–2957, Jun. 2014.
- [7] T. Shan, S. Liu, Y. D. Zhang, M. G. Amin, R. Tao, and Y. Feng
Efficient architecture and hardware implementation of coherent integration processor for digital video broadcast-based passive bistatic radar
IET Radar, Sonar Navig., vol. 10, no. 1, pp. 97–106, 2016.
- [8] Q. He and R. S. Blum
The significant gains from optimally processed multiple signals of opportunity and multiple receive stations in passive radar
IEEE Signal Process. Lett., vol. 21, no. 2, pp. 180–184, Feb. 2014.
- [9] J. Liu, H. Li, and B. Himed
Two target detection algorithms for passive multistatic radar
IEEE Trans. Signal Process., vol. 62, no. 22, pp. 5930–5939, Nov. 2014.
- [10] Q. He, J. Hu, R. S. Blum, and Y. Wu
Generalized Cramér-Rao bound for joint estimation of target position and velocity for active and passive radar networks
IEEE Trans. Signal Process., vol. 64, no. 8, pp. 2078–2089, Apr. 2016.
- [11] H. D. Griffiths and C. J. Baker
Passive coherent location radar systems. Part 1: Performance prediction
IEE Proc. Radar, Sonar Navig., vol. 152, no. 3, pp. 124–132, Jun. 2005.
- [12] C. J. Baker, H. D. Griffiths, and I. Papoutsis
Passive coherent location radar systems. Part 2: Waveform properties
IEE Proc. Radar, Sonar Navig., vol. 152, no. 3, pp. 160–168, Jun. 2005.
- [13] P. E. Howland, D. Maksimiuk, and G. Reitsma
FM radio based bistatic radar
IEE Proc. Radar, Sonar Navig., vol. 152, no. 3, pp. 107–115, Jun. 2005.
- [14] M. K. Baczyk and M. Malanowski
Reconstruction of the reference signal in DVB-T based passive radar
Int. J. Electron. Telecommun., vol. 57, no. 1, pp. 43–48, Mar. 2011.
- [15] J. Liu, H. Li, and B. Himed
On the performance of the cross-correlation detector for passive radar applications
Signal Process., vol. 113, pp. 32–37, 2015.
- [16] D. E. Hack, L. K. Patton, B. Himed, and M. A. Saville
Detection in passive MIMO radar networks
IEEE Trans. Signal Process., vol. 62, no. 11, pp. 2999–3012, Jun. 2014.
- [17] G. Cui, J. Liu, H. Li, and B. Himed
Signal detection with noisy reference for passive sensing
Signal Process., vol. 108, pp. 389–399, Mar. 2015.
- [18] X. Zhang, H. Li, J. Liu, and B. Himed
Joint delay and Doppler estimation for passive sensing with direct-path interference
IEEE Trans. Signal Process., vol. 64, no. 3, pp. 630–640, Feb. 2016.
- [19] O. Rabaste and D. Poullin
Rejection of Doppler shifted multipaths in airborne passive radar
In *Proc. IEEE Int. Radar Conf.*, Arlington, VA, May 2015, pp. 1660–1665.
- [20] D. K. P. Tan, M. Lesturgie, H. Sun, and Y. Lu
Target detection performance analysis for airborne passive bistatic radar
In *Proc. IEEE Int. Geosci. Remote Sens. Symp.*, Jul. 2010, pp. 3553–3556.
- [21] R. Tao, H. Z. Wu, and T. Shan
Direct-path suppression by spatial filtering in digital television terrestrial broadcasting-based passive radar
IET Radar, Sonar Navig., vol. 4, no. 6, pp. 791–805, Dec. 2010.
- [22] J. E. Palmer and S. J. Searle
Evaluation of adaptive filter algorithms for clutter cancellation in passive bistatic radar
In *Proc. IEEE Radar Conf.*, Atlanta, GA, May 2012, pp. 0493–0498.
- [23] F. Colone, R. Cardinali, and P. Lombardo
Cancellation of clutter and multipath in passive radar using a sequential approach
In *Proc. IEEE Conf. Radar*, Verona, NY, Apr. 2006, pp. 393–399.
- [24] F. Colone
et al. Space-time constant modulus algorithm for multipath removal on the reference signal exploited by passive bistatic radar
IET Radar, Sonar Navig., vol. 3, no. 3, pp. 253–264, Jun. 2009.
- [25] Y. Ma, T. Shan, Y. D. Zhang, M. G. Amin, R. Tao, and Y. Feng
A novel two-dimensional sparse-weight NLMS filtering scheme for passive bistatic radar
IEEE Geosci. Remote Sens. Lett., vol. 13, no. 5, pp. 676–680, May 2016.
- [26] M. Feder and E. Weinstein
Parameter estimation of superimposed signals using the EM algorithm
IEEE Trans. Acoust., Speech Signal Process., vol. 36, no. 4, pp. 477–489, Apr. 1988.
- [27] D. E. Hack, L. K. Patton, B. Himed, and M. A. Saville
Centralized passive MIMO radar detection without direct-path reference signals
IEEE Trans. Signal Process., vol. 62, no. 11, pp. 3013–3023, Jun. 2014.
- [28] S. M. Kay
Modern Spectral Estimation: Theory and Application. Englewood Cliffs, NJ, USA: Prentice-Hall, 1988.
- [29] P. Wang, H. Li, and B. Himed
A parametric moving target detector for distributed MIMO radar in non-homogeneous environment
IEEE Trans. Signal Process., vol. 61, no. 9, pp. 2282–2294, May 2013.
- [30] S. M. Kay
Fundamentals of Statistical Signal Processing: Estimation Theory. Upper Saddle River, NJ, USA: Prentice-Hall, 1993.
- [31] M. A. Richards
Fundamentals of Radar Signal Processing. New York, NY, USA: McGraw-Hill, 2005.
- [32] A. Zaimbashi, M. Derakhtian, and A. Sheikhi
Invariant target detection in multiband FM-based passive bistatic radar
IEEE Trans. Aerosp. Electron. Syst., vol. 50, no. 1, pp. 720–736, Jan. 2014.
- [33] Y. Fu, X. Wan, X. Zhang, G. Fang, and J. Yi
Side peak interference mitigation in FM-based passive radar via detection identification
IEEE Trans. Aerosp. Electron. Syst., vol. 53, no. 2, pp. 778–788, Apr. 2017.



Fangzhou Wang received the B.S. and M.S. degrees in electrical engineering from Beijing Institute of Technology, Beijing, China, in 2012 and 2015, respectively. He is currently working toward the Ph.D. degree in electrical engineering at Stevens Institute of Technology, Hoboken, NJ, USA.

He has been a Teaching and Research Assistant with the Department of Electrical and Computer Engineering, Stevens Institute of Technology, since 2015. His research interests include array signal processing, passive sensing, and joint optimization of communication-sensing systems.



Hongbin Li (M'99–SM'08) received the B.S. and M.S. degrees from the University of Electronic Science and Technology of China, Chengdu, China, and the Ph.D. degree from the University of Florida, Gainesville, FL, USA, in 1991, 1994, and 1999, respectively, all in electrical engineering.

From July 1996 to May 1999, he was a Research Assistant with the Department of Electrical and Computer Engineering, University of Florida. Since July 1999, he has been with the Department of Electrical and Computer Engineering, Stevens Institute of Technology, Hoboken, NJ, USA, where he became a Professor in 2010. He was a Summer Visiting Faculty Member with the Air Force Research Laboratory in the summers of 2003, 2004, and 2009. His research interests include statistical signal processing, wireless communications, and radars.

Dr. Li has been a member of the IEEE SPS Signal Processing Theory and Methods Technical Committee (TC) and the IEEE SPS Sensor Array and Multichannel TC, an Associate Editor for *Signal Processing* (Elsevier), the IEEE TRANSACTIONS ON SIGNAL PROCESSING, the IEEE SIGNAL PROCESSING LETTERS, and the IEEE TRANSACTIONS ON WIRELESS COMMUNICATIONS, as well as a Guest Editor for the IEEE JOURNAL OF SELECTED TOPICS IN SIGNAL PROCESSING and the *EURASIP Journal on Applied Signal Processing*. He has been involved in various conference organization activities, including serving as a General Co-Chair for the 7th IEEE Sensor Array and Multichannel Signal Processing Workshop, Hoboken, NJ, June 17–20, 2012. He is the recipient of the IEEE Jack Neubauer Memorial Award in 2013 from the IEEE Vehicular Technology Society, the Outstanding Paper Award from the IEEE AFICON Conference in 2011, the Harvey N. Davis Teaching Award in 2003 and the Jess H. Davis Memorial Award for excellence in research in 2001 from Stevens Institute of Technology, and the Sigma Xi Graduate Research Award from the University of Florida in 1999. He is a member of Tau Beta Pi and Phi Kappa Phi.



Xin Zhang (S'17–M'17) received the B.Eng. degree (with honors) from the University of Science and Technology Beijing, Beijing, China, the M.Eng. degree from the Beijing University of Posts and Telecommunications, Beijing, China, and the Ph.D. degree from Stevens Institute of Technology (SIT), Hoboken, NJ, USA, in 2008, 2011, and May 2017, respectively, all in electrical engineering.

From 2011 to 2017, he worked as a Research and Teaching Assistant with the Signal Processing and Communication Laboratory, Department of Electrical and Computer Engineering, SIT. He is currently a Senior RF Application Engineer with LitePoint, a Teradyne company, in Sunnyvale, CA, USA. His research interests include statistical signal processing, optimization algorithm applications, passive sensing, and wireless communications.



Braham Himed (F'14) received the Engineering degree from Ecole Nationale Polytechnique of Algiers, El Harrach, Algeria, and the M.S. and Ph.D. degrees from Syracuse University, Syracuse, NY, USA, in 1984, 1987, and 1990, respectively, all in electrical engineering.

He is a Technical Advisor with the Sensors Directorate, RF Technology Branch, Air Force Research Laboratory (AFRL), Dayton, OH, USA, where he is involved with several aspects of radar developments. His research interests include detection, estimation, multichannel adaptive signal processing, time series analyses, array processing, adaptive processing, waveform diversity, distributed active/passive radar, and over the horizon radar.

Dr. Himed is the Chair of the AES Radar Systems Panel. He is also a Fellow of AFRL (class of 2013). He is the recipient of the 2001 IEEE region I award for his work on bistatic radar systems, algorithm development, and phenomenology, and the 2012 IEEE Warren White award for excellence in radar engineering.